

FORM 10/64 04-106
ESTI FILE COPY

VULNERABILITY OF MANNED ORBITAL COMMAND POSTS TO NATURAL SPACE RADIATIONS

TECHNICAL DOCUMENTARY REPORT NO. ESD-TDR-64-164

NOVEMBER 1964

F. W. French and K. F. Hansen

Prepared for

DIRECTORATE OF SPECIAL SYSTEMS

ELECTRONIC SYSTEMS DIVISION

AIR FORCE SYSTEMS COMMAND

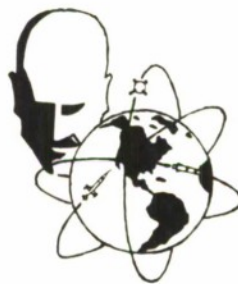
UNITED STATES AIR FORCE

L. G. Hanscom Field, Bedford, Massachusetts

ESD RECORD COPY

RETURN TO
SCIENTIFIC & TECHNICAL INFORMATION DIVISION
(ESTI), BUILDING 1211

COPY NR. _____ OF _____ COPIES



Project 611. 1

Prepared by

THE MITRE CORPORATION
Bedford, Massachusetts
Contract AF19(628)-2390

ESTI PROCESSED

DDC TAB PROJ OFFICER

ACCESSION MASTER FILE

DATE _____

ESTI CONTROL NR. AL 44209

CY NR. 1 OF 1 CYS

ADD009501

Copies available at Office of Technical Services,
Department of Commerce.

Qualified requesters may obtain copies from DDC.
Orders will be expedited if placed through the librarian
or other person designated to request documents
from DDC.

When US Government drawings, specifications, or
other data are used for any purpose other than a
definitely related government procurement operation,
the government thereby incurs no responsibility
nor any obligation whatsoever; and the fact that the
government may have formulated, furnished, or in
any way supplied the said drawings, specifications,
or other data is not to be regarded by implication
or otherwise, as in any manner licensing the holder
or any other person or corporation, or conveying
any rights or permission to manufacture, use, or sell
any patented invention that may in any way be related
thereto.

Do not return this copy. Retain or destroy.

VULNERABILITY OF MANNED ORBITAL COMMAND
POSTS TO NATURAL SPACE RADIATIONS

TECHNICAL DOCUMENTARY REPORT NO. ESD-TDR-64-164

NOVEMBER 1964

F. W. French and K. F. Hansen

Prepared for

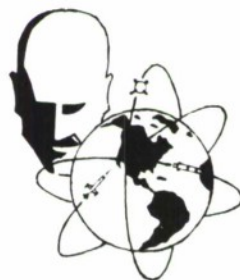
DIRECTORATE OF SPECIAL SYSTEMS

ELECTRONIC SYSTEMS DIVISION

AIR FORCE SYSTEMS COMMAND

UNITED STATES AIR FORCE

L. G. Hanscom Field, Bedford, Massachusetts



Project 611. 1

Prepared by

THE MITRE CORPORATION

Bedford, Massachusetts

Contract AF19(628)-2390

FOREWORD

The authors would like to thank Col. J. E. Pickering and Maj. D. Anderson of the Air Force Aerospace Medical Division, and J. Billingham and J. Modisette of the NASA Manned Spacecraft Center for helpful background discussions on radiobiological effects and on the radiation environment. We should also like to thank L. Leist of Department 51 for carrying out the programming for the shielding calculations.

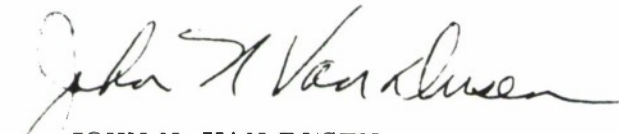
ABSTRACT

The shielding requirements for the protection of the crew of a manned orbital command post against the natural space radiations are investigated. Two types of orbits of military importance and of wide applicability are considered--a long-duration, high-altitude orbit above the Van Allen Belt and a short-duration, low-altitude polar orbit below it. Model environments for both orbits in terms of solar flare, cosmic, and Van Allen Belt radiations are postulated. Radiobiological tolerance criteria are investigated, and a somewhat unique criteria, based on partial recovery of sustained somatic damage, is proposed for the long duration mission.

A mathematical description of the radiation transport of the separate environmental components through the radiation shield is formulated. Appropriate simplifications are used to obtain expressions for the doses due to primary protons, secondary protons and neutrons, and bremsstrahlung. Calculations are carried out on the IBM 7030 computer to obtain dose vs. thickness curves for different types and amounts of shielding material. These curves, together with the assumed model environment, and the postulated radiobiological tolerance criteria, are used to calculate minimum shielding thicknesses for both types of orbits. Conclusions are then drawn on the total amount of radiation shielding material that must be carried for each orbit.

REVIEW AND APPROVAL

Publication of this technical documentary report does not constitute Air Force approval of the reports findings or conclusions. It is published only for the exchange and stimulation of ideas.



JOHN N. VAN DUSEN
Major USAF

TABLE OF CONTENTS

SECTION		<u>Page</u>
I	INTRODUCTION	1
II	MISSION PROFILES AND VEHICLE CONFIGURATION	3
	HIGH-ALTITUDE ORBIT MISSION PROFILE	3
	LOW-ALTITUDE ORBIT MISSION PROFILE	4
	VEHICLE CONFIGURATION	4
III	MODEL ENVIRONMENT	7
	HIGH-ALTITUDE ORBIT ENVIRONMENT	7
	Solar Flares	7
	Van Allen Belt	14
	Cosmic Rays	21
	LOW-ALTITUDE ORBIT ENVIRONMENT	21
	Geomagnetic Field Effects	21
	Solar Flares	22
	Cosmic Rays	23
IV	RADIOBIOLOGICAL TOLERANCE CRITERIA	25
	GENERAL CONSIDERATIONS	25
	HIGH-ALTITUDE ORBIT TOLERANCE CRITERION	26
	Analytic Formulation	27
	Quantitative Criteria	28
	LOW-ALTITUDE ORBIT TOLERANCE CRITERION	30
V	SHIELDING CALCULATIONS	31
VI	RESULTS AND DISCUSSION	33
	GENERAL	33
	HIGH-ALTITUDE ORBIT	38

TABLE OF CONTENTS (CONT.)

SECTION		<u>Page</u>
VI (cont'd)	LOW-ALTITUDE ORBIT	40
	TOTAL SHIELD WEIGHTS	42
APPENDIXES		
I	CALCULATION OF RADIATION DOSES	47
	PRIMARY PROTON DOSES	47
	SECONDARY PROTON DOSES	52
	SECONDARY NEUTRON DOSES	56
	ELECTRON DOSES	60
II	POLAR ORBIT DOSES	63
	REFERENCES	69

LIST OF ILLUSTRATIONS

	<u>Title</u>	<u>Page</u>
Fig. 1	Altitude vs Time During Transfer From Parking to High-Altitude Orbit	15
Fig. 2	Integrated Proton Flux in the Van Allen Belt vs Altitude	16
Fig. 3	Nondimensional Integrated Proton Flux in the Van Allen Belt vs Transfer Time	17
Fig. 4	Integral Electron Flux Spectra in the Van Allen Belt	18
Fig. 5	Integrated Electron Flux in the Van Allen Belt vs Altitude	20
Fig. 6	Nondimensional Integrated Electron Flux in the Van Allen Belt vs Transfer Time	20
Fig. 7	Dose vs Shield Thickness for May 10, 1959 (Type A) Flare (High-Altitude Orbit)	33
Fig. 8	Dose vs Shield Thickness for November 12-15, 1960 (Type B) Flare Sequence (High-Altitude Orbit)	34
Fig. 9	Dose vs Shield Thickness for February 23, 1956 Flare (High-Altitude Orbit)	34
Fig. 10	Dose vs Shield Thickness for Passage Through the Van Allen Belt (High-Altitude Orbit)	35
Fig. 11	Primary Proton Dose vs Shield Thickness for three Major Solar Flares (Low-Altitude Polar Orbit)	35
Fig. 12	Secondary Dose vs Shield Thickness for November 12-15, 1960 Flare Sequence (High-Altitude Orbit)	36
Fig. 13	Effective Dose vs Time (High-Altitude Orbit)	36
Fig. 14	Ratio of Polar Orbit to Free Space Dose vs Shield Thickness for 3 Major Solar Flares (Using Simple Dipole Geomagnetic Field)	41
Fig. 15	Shell Geometry	48

LIST OF ILLUSTRATIONS (CONT.)

		<u>Page</u>
Fig. 16	Bremsstrahlung Source Surface	61
Fig. 17	Modification of Geomagnetic Field During Solar Flare	64

LIST OF TABLES

Table 1	J _o and R _o Values for November 12-15, 1960 and May 10, 1959 Flares	11
Table 2	Constants for February 23, 1956 Flare	14
Table 3	Dose Rate Per Unit Mass Per Unit Flux	51
Table 4	Number and Energy of Cascade Protons	55
Table 5	Proton Inelastic Cross-Sections	55
Table 6	Mean Number of Cascade and Evaporation Neutrons per Inelastic Collision	59
Table 7	Neutron Doses per Unit Flux as a Function of Neutron Energy	59

SECTION I

INTRODUCTION

It is vital to our national defense posture to always maintain effective command and control over our global strike forces. This requires that we have command posts that are survivable in the event of a surprise attack. As pointed out by General Power,^[1] a promising method of attaining such survivability is through the use of maneuverable command posts in space.

Over the past several years, the merits of various types of manned orbital command posts (MOCOPs) have been investigated. The vulnerability of such vehicles to direct nuclear attack has been reported previously.^[2] In investigating the feasibility of such vehicles, one of the most important considerations is the protection required to make them survivable in the natural space environment.

Perhaps the most important component of the space environment for manned space flight is the charged particle radiations. These radiations may be divided into the three following types: Van Allen Belt radiations (protons and electrons trapped in the geomagnetic field); solar flare radiations (transient, energetic proton streams, associated with flares on the sun); and cosmic radiations (protons and heavier ions which arrive from all directions of our galaxy). Because of the biological effects produced on the crew by these radiations, shielding must be employed in the space vehicle to attenuate the radiations. For certain types of orbits and boosters available in a given time period, the amount of shielding required to give even minimum protection to the crew may so severely limit the payload as to render the mission infeasible. For this reason,

evaluation of the merit and feasibility of proposed types of command and control missions in space necessitates careful investigation of radiation protection requirements.

The general problem of the vulnerability of MOCOPs to space radiations is investigated by considering two specific types of orbits. The first is a high-altitude (50,000 n. m.) orbit and the second is a low-altitude (200 n. m.) polar orbit. These orbits were chosen both because of their military significance and because each one is representative of a class of radiation vulnerability problem. The results that are obtained in this study will be applicable to a fairly broad range of orbits. For instance, many of the results for the high-altitude orbit will be applicable to any orbit in cislunar space that is outside the Van Allen Belt most of the time, and even to interplanetary transfers. The results for the low-altitude polar orbit will be applicable to any polar orbit below the Van Allen Belt and will be an upper bound on any nonpolar orbit below the Van Allen Belt.

This paper first discusses the assumed mission profiles and vehicle configuration. The environment models assumed for the missions are then presented. Radiation dose criteria for the crew are next stipulated. The shielding calculations are briefly discussed and are presented in detail in Appendices I and II. Finally, the results of the shielding calculations and the dose criteria are used to determine requisite amounts of shielding.

SECTION II

MISSION PROFILES AND VEHICLE CONFIGURATION

HIGH-ALTITUDE ORBIT MISSION PROFILE

A high-altitude orbit for the MOCOP is attractive because it is difficult for an enemy to successfully launch a surprise attack on it, and also because the MOCOP has considerable maneuvering room to evade enemy detection and/or attack. The orbit should not be so high as to make contact with the earth difficult but should be high enough to be outside of the trapped radiation belt. With these considerations in mind, an operational altitude of 50,000 nautical miles was selected. As the results of the study later showed, the choice of particular orbital altitude is not too important in determining radiation shielding requirements, as long as it is outside the geomagnetic field. The radiation encountered in this orbit is, as far as is known, the same as that encountered everywhere in cislunar space and will be designated as the "free-space" radiation.

It is assumed that the vehicle arrives at the operational altitude by first going into a 100 n. m. parking orbit and then transferring to the higher altitude by means of a Hohmann semi-ellipse. Once the vehicle reaches operational altitude, it is assumed that it is continuously manned by rotating crews. For this type of orbit, it is desirable to keep crew rotations to a minimum. Therefore, extended orbital tours of duty in the range of three months to one year will be considered.

LOW-ALTITUDE ORBIT MISSION PROFILE

While a low-altitude orbit for a MOCOP may be more vulnerable to enemy attack, it does possess several attractive features. For instance, such orbits have less demanding initial and resupply booster requirements than high-altitude orbits, allow observation of the earth in greater detail, and, as will be shown, can permit less stringent radiation shielding requirements. (It is assumed that we are considering a time period in which the geomagnetic field at low altitudes is essentially free of Argus-type electrons.) For MOCOP missions, polar and nearly-polar orbits are of interest because of their earth-coverage properties. Hence, the low-altitude orbit that is considered is the polar circular orbit at a nominal altitude of 200 n. m.

Because of the relative ease of resupply and crew rotation as compared to the high-altitude case, it is envisioned that the orbital tours of duty will be shorter. Therefore, tours of duty in the range from one week to three months will be considered.

VEHICLE CONFIGURATION

For both the high- and low-altitude cases, the MOCOPs are envisioned as one or several identical, semi-independent, rigid modules. Each module is assumed to be cylindrical in shape with a diameter of 12 feet and a length of 25 feet. The effects of the radiations in a typical module are considered by neglecting the interaction between the modules, which is estimated to be small. It is further assumed that the modules have no reentry capability in themselves. Each module consists of an outer cylindrical shell plus an inner, spherical "storm cellar" for protection against severe radiations.

The design of the outer shell is influenced by launch and orbit structural loads as well as micrometeorite protection and thermal balance considerations. It is assumed that the shell is of aluminum-foamed polyurethane-aluminum multiwall construction with a unit weight of 1.5 gm/cm^2 ($\approx 3.1 \text{ lb/ft}^2$). The storm cellar concept for radiation shielding is used to minimize the weight of shielding material and the storm cellar is occupied only in times of severe solar flares and, in the high-altitude orbit case, passage through the Van Allen Belt. Since the time between the observance of the maximum visual flare intensity and the arrival of substantial proton fluxes near the earth is greater than a half-hour, there is adequate time for the crew to retire to the storm cellar.

SECTION III

MODEL ENVIRONMENT

HIGH-ALTITUDE ORBIT ENVIRONMENT

Solar Flares

The current state of knowledge concerning the solar flare phenomenon makes the postulation of a model solar flare environment difficult because of the following basic deficiencies in our knowledge. First, there is little understanding of the mechanism of the genesis of a solar flare and its relation to associated proton streams. Their occurrence seems to follow a random pattern and each flare appears to have its own characteristic time-varying energy spectrum. Second the limited number of observations rule out any meaningful statistical analysis of flares. It has long been known that solar activity follows an 11-year cycle and recent observations indicate that most important solar flares occur before and after the maximum of the cycle. However, the most important data on flares have only been obtained through approximately one solar cycle. Third, even fairly recent observations are often lacking in data at low energies and early times. Hopefully, in the future these three deficiencies will be rectified by continued observations and utilization of data from such special-purpose satellites as OSO and IMP. For the present, one is forced to rely on past observations to hypothesize what solar flare environment will be encountered by future astronauts.

The important solar flares that can deliver a lethal or disabling sublethal dose to a space crew are sometimes categorized as "major" and "giant" events. A major solar flare has a high-flux, low-to-medium energy spectrum. Typical

of the most intense of this type are the May 10, 1959 flare (high flux, low energy) and the November 12, 1960 flare (high flux, medium energy). Major flares occur two to four times a year during periods of increasing or decreasing solar activity; e. g. , 1959 was possibly the worst year for major solar flares as four occurred that would have caused an integrated skin dose in free space of greater than 100 rad behind 1 gm/cm^2 of shielding.^[3,4] Giant solar flares have low or moderate fluxes of extremely high energy (in the relativistic range), and occur maybe once every two years. The classic example of this type is the February 23, 1956 flare, the most energetic ever observed.

Other flares of lesser flux and energy occur much more frequently and it is conceivable that their cumulative effect may be important. However, on the basis of estimates of Reference 3, even if the crew remains outside of the radiation shield during minor flares, they will accumulate a dose of no greater than 12 rad in a year from these flares. For the present study, it is assumed that the crew uses the radiation shield as a shelter against the more important of these minor flares so that the cumulative dose is reduced to a very low value which can be neglected.

The solar flare model environment postulated must be somewhat arbitrary, and hence given to second-guessing. In the last analysis, it must be arrived at by judgment, balancing conservatism against probability. There is no apparent physical reason why six giant flares such as that of February 23, 1956 cannot occur during a twelve month period, but on the basis of past experience such an occurrence seems very unlikely. The present study considers two types of flares: Type A, a high-flux, low-energy flare that is represented by the May 10, 1959 flare; and Type B, (in reality two consecutive, high-flux, medium-energy flares) that is represented by the November 12-15, 1960 sequence. This latter, double-type flare is considered because the radiation damage criteria to be used

is more sensitive to two identical flares occurring consecutively than to two identical flares occurring several months apart. These particular flares were chosen for the model environment because they are among the most intense of their types and because fairly good data exists on their behavior.

Orbital tours of duty of from three months to one year are considered and the assumed time-phasing of the flares is shown below for 3-, 6-, and 12-month missions.

	1	2	3	4	5	6	7	8	9	10	11	12
12 month mission		A				B				A		
6 month mission		A				B						
3 month mission			B									

A = May 10, 1959 flare

B = November 12-15, 1960 flare sequence

The environment is specified in terms of A- and B-type flares, but the results will be analyzed to obtain the effect of substituting a February 23, 1956 type flare for an A or B type.

Having selected the flares to be used in the model environment, the problem arises as how best to represent the flare behavior analytically. After some consideration, it was decided to use, wherever possible, the exponential rigidity formulation proposed by Freier and Webber.^[5, 3] This is a one parameter spectrum of the form

$$J = J_0(t) e^{-R/R_0(t)} \quad (1)$$

where

J = integral proton flux with rigidity greater than R
(protons/cm² sec ster)

R = proton rigidity (momentum per unit charge)

J_0 = total integral proton flux ($R > 0$)

R_0 = characteristic rigidity (for a given time in a given event)

Specific analytical representation of the May 10, 1959, November 12-15, 1960, and the February 23, 1956 flares are discussed below.

November 12-15, 1960 Flare Sequence

Values of $J_0(t)$ and $R_0(t)$ are taken directly from Reference 5 and are presented in Table 1.

May 10, 1959 Flare

Values of $J_0(t)$ and $R_0(t)$ from $t_{o.m.} + 32$ hours onward, where $t_{o.m.}$ is the time of optical maximum, are given in Table 1⁽⁵⁾. Values of $R_0(t)$ between $t = t_{o.m.}$ and $t = t_{o.m.} + 32$ hours are obtained by extrapolation of the tabulated values of R_0 for $t > 32$ hours. Values of $J_0(t)$ between $t = t_{o.m.}$ and $t = t_{o.m.} + 32$ hours are obtained by assuming that J_0 rose linearly for 20 hours (based on data in References 3 and 4) until it reached the value of J_0 at $t = t_{o.m.} + 32$ hours. J_0 is taken constant between 20 and 32 hours.

February 23, 1956 Flare

Analytic representation of this flare is hampered by lack of observational data. Sufficient data does not exist to represent this flare in terms of exponential rigidity spectra so that a formulation commensurate with available data is necessary.

Table 1

J_o and R_o Values for November 12-15, 1960 and May 10, 1959 Flares*

Date of Solar Flare	Time of Optical Maximum	Time of Measurement	J_o , protons/ c_m^2 sec ster	R_o , Mv		
May 10, 1959	2118	5/12 0500	30×10^3	65		
		0520 } 0915 }	18×10^3	70		
		0915 } 1335 }	4.1×10^3	70		
		1335 } 1750 }	2.8×10^3	66		
November 12, 1960	1329	11/12 1930	1100	280		
		2000	1250	240		
		11/13 0200	3400	185		
		0800	3400	155		
		1305	3000	120		
		1830 } 2000 }	2800	95		
		2230	1000	105		
		11/14 0500	1000	95		
		November 15, 1960	0221	11/15 0500	250	375
				1130	320	240
1030 } 1230 }	285			175		
2130	3300			120		
11/16 0930	1000			100		
1430 } 1730 }	300			100		

* (From Table 2 of Reference 5)

It is assumed^[3, 4] that for a given energy E_1 the timewise variation in integral proton flux is given by

$$J(t, E > E_1) = J_{\max}(E > E_1) e^{-t/t_D(E_1)} \quad (2)$$

where

$J_{\max}(E > E_1)$ = timewise maximum integral flux

t = time measured from maximum flux

$t_D(E_1)$ = characteristic decay time (which is a function of energy)

Integral energy flux spectra (J versus E) are given by Foelsche^[6] for prompt and 19-hour conditions. Because of the extreme energy of this flare, the rise time is short, so the assumption is made that the rise time is zero, and that the prompt spectrum represents the maximum flux condition. Then, with the prompt and 19-hour spectra data from Reference 6, Eq. (2) can be used to obtain $t_D(E)$.

It is assumed that the differential energy spectrum follows a piecewise power law, and for the i^{th} interval has the form

$$\varphi_i(E) = C_i e^{-t/t_{D,i}(E)} E^{-n_i} \quad (E_i \leq E \leq E_{i+1}) \quad (3)$$

where

φ_i = differential proton flux in i^{th} interval

C_i, n_i = constants in i^{th} interval

The integral proton flux J_i can be obtained by integration of Eq. (3). At $t = 0$ this is

$$J(E > E_i) = J(E > E_{i+1}) + \frac{C_i}{n_i - 1} \left(E_i^{1-n_i} - E_{i+1}^{1-n_i} \right) \quad (4)$$

One can then also write

$$\frac{J(E > E_j) - J(E > E_{i+1})}{J(E > E_i) - J(E > E_{i+1})} = \frac{E_j^{1-n_i} - E_{i+1}^{1-n_i}}{E_i^{1-n_i} - E_{i+1}^{1-n_i}} \quad (5)$$

where $E_i < E_j < E_{i+1}$

Values of n_i can be obtained from a given integral energy prompt spectrum by reading off values of J and E at the end points (corresponding to E_i and E_{i+1}) and an intermediate point (corresponding to E_j) of the various intervals, and then applying Eq. (5). With n_i determined, Eq. (4) may be used to calculate the various C_i .

The procedure just indicated is applied to the data of Reference 6 to calculate the quantities C_i , t_{D_i} , and n_i in Eq. (3) that define the spectrum. The results are given in Table 2. It should be emphasized that because of the scarcity of data on this flare, and the resultant assumptions and extrapolations that were necessary to represent its behavior, the confidence level in the representation is lower than for the A- and B-type flares.

Table 2

Constants for February 23, 1956 Flare

Interval Number	Energy Range, Mev.	t_{D_i} , hr	n_i	C_i , $\text{cm}^{-2} \text{sec}^{-1} \text{ster}^{-1} \text{Mev}^{n_i-1}$
1	20 - 100	4.8	1.0	4.66×10^3
2	100 - 160	4.4	1.0	4.68×10^3
3	160 - 300	3.6	1.08	5.14×10^3
4	300 - 550	2.9	2.16	2.75×10^6
5	550 - 1,600	2.3	2.37	3.06×10^7
6	1,600 - 5,000	1.65	5.21	7.57×10^{16}
7	5,000 - 10,000	1.65	7.59	3.93×10^{25}

Van Allen Belt

It is assumed that the traversal of the Van Allen Belt from parking in high-altitude orbit, and vice versa, is made in the plane of the geomagnetic equator. Orientation of the transfer trajectory in this plane will result in a maximum dose and thus furnish an upper limit on the trapped particle dose. A Hohmann semi-ellipse is chosen for the transfer trajectory, giving a transit time of 16.7 hours. The result of calculations carried out to determine the vehicle's altitude as a function of time during the transfer is shown in Fig. 1.

Proton Flux

Several proposed curves of differential proton energy spectra in the heart of the inner belt are given in Fig. 3-2 of Reference 7. The recommendation therein to use the curve based on Lockheed HEPDEX and LEPDEX⁽⁸⁾ data is followed: This spectrum is defined as

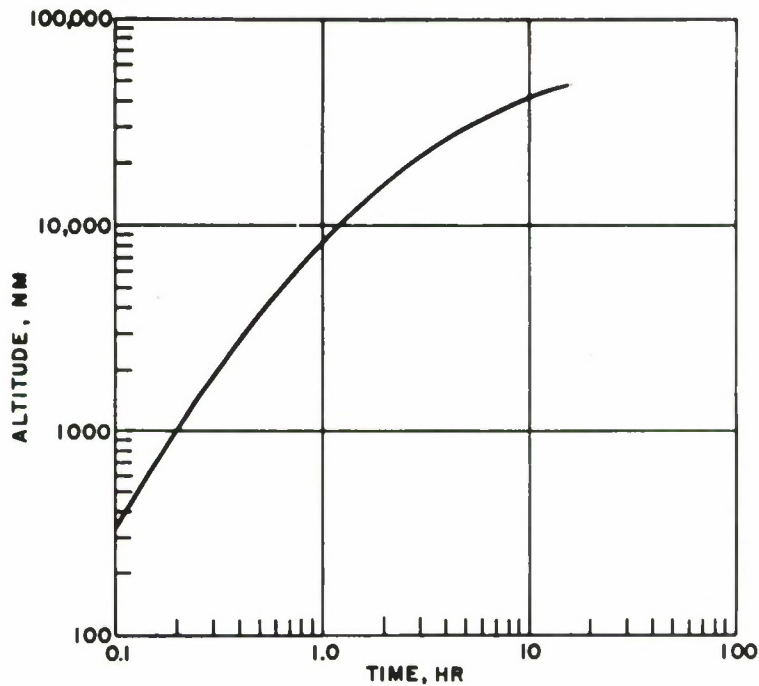


Fig. 1. Altitude vs Time During Transfer From Parking to High-Altitude Orbit

$$\begin{aligned} \varphi &= 5.33 \times 10^3 \text{ protons/cm}^2\text{-sec-Mev} & E < 30 \text{ Mev} \\ \varphi &= 1.44 \times 10^8 E^{-3.0} \text{ protons/cm}^2\text{-sec-Mev} & E > 30 \text{ Mev} \end{aligned} \quad (6)$$

For the present investigation, it is assumed that this spectrum is invariant with altitude. A curve of integrated proton flux ($E > 30$ Mev) versus altitude, based on Explorer IV, Pioneer III, and HEPDEX data^[8] from Fig. 3-3 of Reference 7 is shown in Fig. 2.

Note that the dose rate behind a shield is proportional to φ , and consequently to J . Let the dose rate behind a given shield in the heart of the inner belt be denoted by $D(h_{\text{ref.}})$. Then at any other altitude:

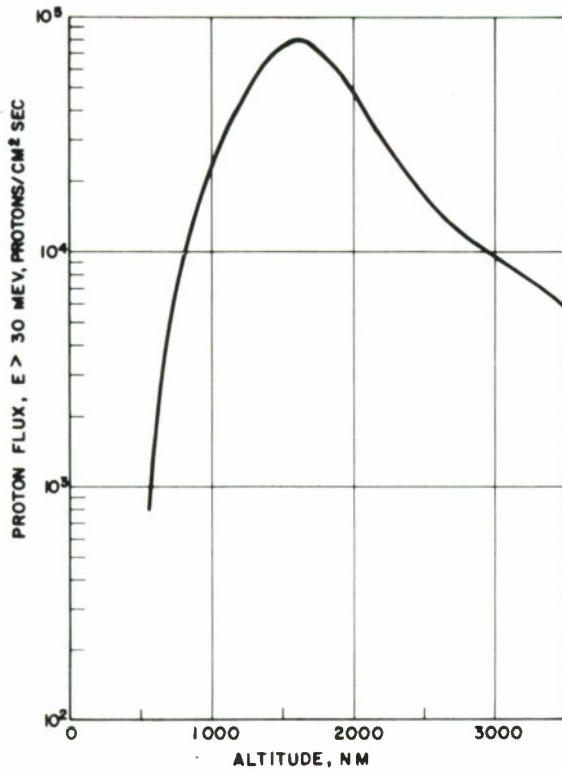


Fig. 2. Integrated Proton Flux in the Van Allen Belt vs Altitude

$$\dot{D}(h) = \dot{D}(h_{\text{ref}}) \frac{J(h, E > 30)}{J(h_{\text{ref}}, E > 30)} \quad (7)$$

where

h_{ref} = reference altitude = altitude at peak of inner belt

$J(h, E > 30)$ = integral flux at altitude h as obtained from Fig. 2

$J(h_{\text{ref}}, E > 30)$ = integral flux at reference altitude as obtained from Fig. 2.

The total proton dose, D received during transit is

$$D = \int_0^T \dot{D}(t) dt = \dot{D}(h_{\text{ref}}) \int_0^T \frac{J(h, E > 30)}{J(h_{\text{ref}}, E > 30)} dt \quad (8)$$

where

τ = transit time

One can combine the curve of h versus t from Fig. 1 with the curve of $J(E > 30)$ versus h in Fig. 2, to obtain the curve of $J(E > 30)/J_{\text{ref}}(E > 30)$ versus t in Fig. 3. Numerical integration of this curve, in accordance with Eq. (8), then leads to

$$D = T_p^* \dot{D}(h_{\text{ref}}) \quad (9)$$

where T_p^* is the integral in the right-hand expression in Eq. (8). Equation (9) may be interpreted as the proton dose received during the transfer trajectory equals the product of the dose rate received in the heart of the inner belt and a fictitious time T_p^* .

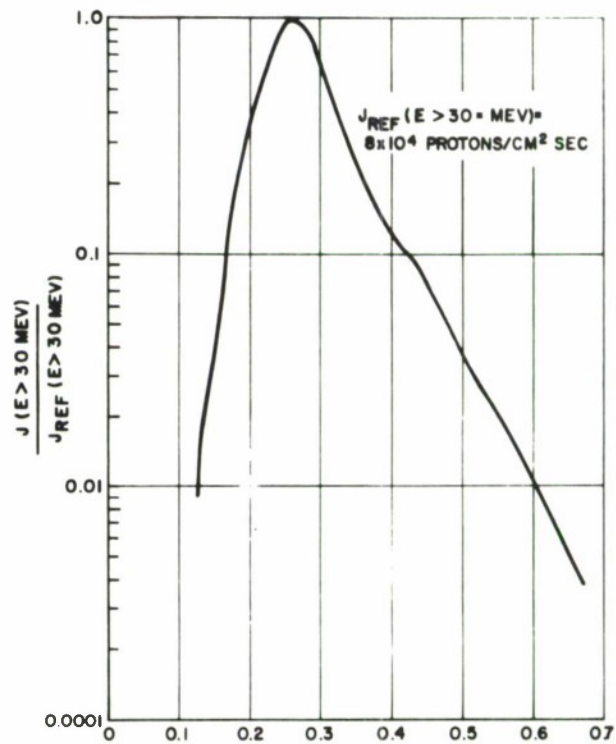


Fig. 3. Nondimensional Integrated Proton Flux in the Van Allen Belt vs Transfer Time

The above formulation of the problem requires only one shielding calculation for a given shield configuration. This calculation is carried out for the peak flux and the result is multiplied by the factor $T_p^* = 0.128$ hour to yield the proton dose during orbit transfer. For other transfer trajectories, the same computational procedure can be followed with appropriate values of T_p^* .

Electrons

The undisturbed electron spectra encountered by the vehicle in passing through the Van Allen Belt is formulated in a manner similar to that used for the Van Allen proton spectra previously described. In this case, it is assumed that there are two invariant spectra--one for the inner belt and one for the outer belt. The assumed spectra are shown in Fig. 4, as taken from Reference 9, the

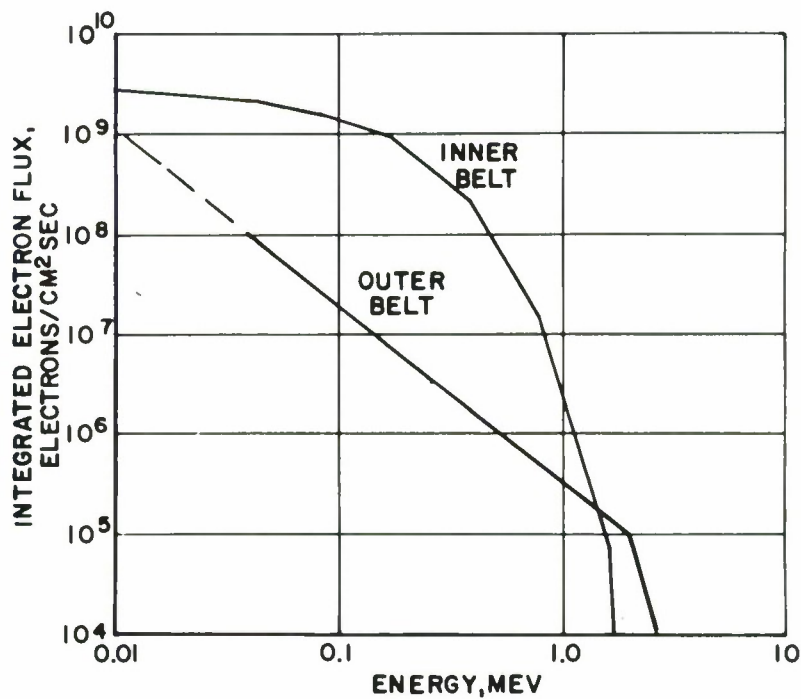


Fig. 4. Integral Electron Flux Spectra in the Van Allen Belt

inner belt spectra being that given in Reference 10 and the outer belt that given by Van Allen in the symposium, **Space Flight Report to the Nation**. Also presented in Reference 9 are data from which it is possible to construct the curve of integral electron flux ($E > 20$ kev) versus altitude that is shown in Fig. 5.

Preliminary shielding calculations showed that the dose due to the electrons could be ignored compared to that due to their bremsstrahlung, so that only the latter is considered here.

Calculation of the bremsstrahlung dose is carried out in a manner analogous to that described in the previous section for the protons, except that separate integrations are carried out over the inner and outer belts. Therefore, analogous to Eqs. (8) and (9), there are

$$D_e = \dot{D}_{e, i_{ref}} \int \frac{J_e(t)}{J_{e, i_{ref}}} dt \Big]_{inner} \tag{10}$$

$$+ \dot{D}_{e, o_{ref}} \int \frac{J_e(t)}{J_{e, o_{ref}}} dt \Big]_{outer}$$

$$D_e = \dot{D}_{e, i_{ref}} T^*_{e, i} + \dot{D}_{e, o_{ref}} T^*_{e, o} \tag{11}$$

where the subscript e denotes electron, and the subscripts i and o denote inner and outer belt, respectively. Figures 4 and 5 can then be combined to obtain the curve of $J_e/J_{e_{ref}}$ shown in Fig. 6. Numerical integration of Fig. 6

yields $T^*_{e, i} = 0.919$ hour and $T^*_{e, o} = 0.607$ hour.

Fig. 5. Integrated Electron Flux in the Van Allen Belt vs Altitude

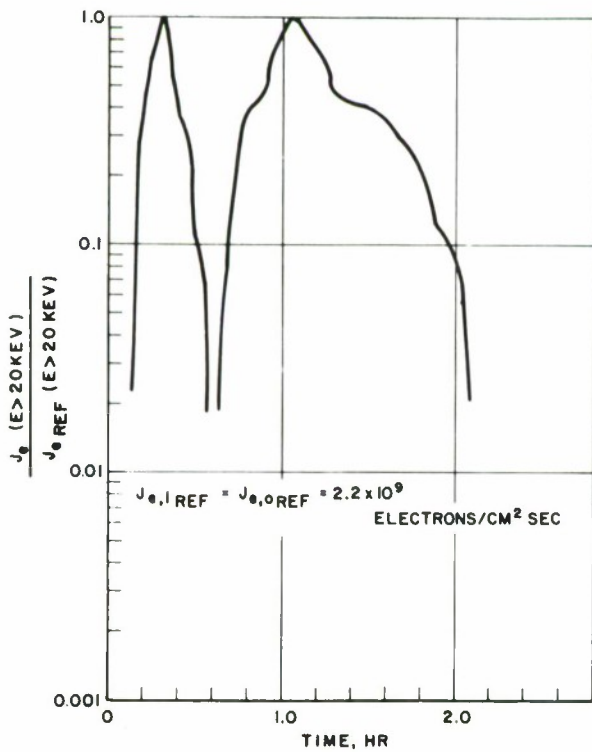
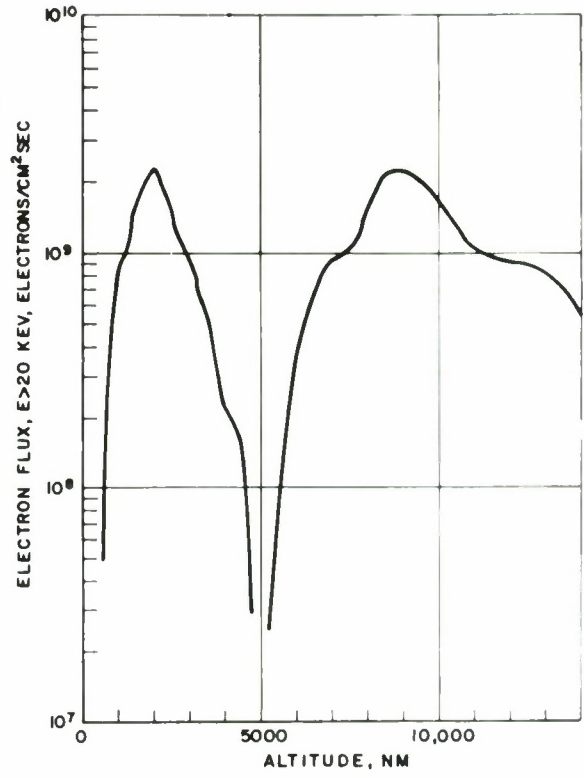


Fig. 6. Nondimensional Integrated Electron Flux in the Van Allen Belt vs Transfer Time

Cosmic Rays

It is assumed that except during periods of major and giant solar flares, the normal on-orbit operating mode of the crew is outside the storm cellar. Hence, during most of their duty tour, the crew will be subjected to the effects of the background cosmic radiation (or galactic cosmic radiation) shielded only by the wall of the space vehicle. These radiations are of such high energy that the vehicle's wall will not significantly attenuate them, and the dose received inside the cabin will be essentially unshielded.

While the spectrum and composition of the cosmic rays are thought to be known fairly well (e. g. , References 11, 12), the biological effects of the high-energy protons and the heavy primaries are at present poorly understood. In view of this latter uncertainty, it is inconsistent to use a detailed cosmic ray spectrum in the shielding calculations. Instead, the unshielded dose rate of 26 rem/yr proposed by Tobias^[13] will be accepted.

LOW-ALTITUDE ORBIT ENVIRONMENT

Geomagnetic Field Effects

The only radiation components encountered by a vehicle in the low-altitude orbit are those of solar flares and cosmic rays, since the orbital altitude is below the Van Allen Belt. The main difference in radiation environment encountered in this orbit and that encountered in the high-altitude orbit is due to the filtering action of the geomagnetic field on charged particles.* This effect

*There is another difference between the high- and low-altitude radiation environments that was not considered in the present study because of lack of information, and because its neglect errs on the conservative side. This difference is that, due to the shielding action of the earth, the incident radiations may not be isotropic in low-altitude orbits. It is not possible to estimate the importance of this effect, but an upper bound is that it reduces the flux by one half.

is a function of geomagnetic latitude and for each latitude there is a corresponding minimum rigidity (cutoff rigidity) that a charged particle must possess to penetrate this field. The cutoff rigidity varies from about 14.9 Bev/C (see Appendix II) at the geomagnetic equator to what is thought to be about zero at the geomagnetic poles for normally incident particles. Thus, a vehicle in an orbit in the plane of the geomagnetic poles receives a variable dose rate, even if the free-space dose rate is constant. The dose rate during orbit will be the free-space dose rate when the vehicle is over either of the geomagnetic poles and close to zero when it is in the equatorial regions. For a given (low) altitude, such a vehicle will receive a maximum dose rate as compared to vehicles in orbits with different inclinations. Since the geomagnetic and geographic poles are fairly close (the geomagnetic north pole is at 78.5° N latitude), the dose received during a geomagnetic polar orbit should furnish a fairly close and conservative estimate of that received during a geographical polar orbit. Because of the much greater computational simplicity in calculating the radiation dose in a geomagnetic polar orbit, as compared to geographical polar orbit, the radiation environment assumed for the low-altitude orbit is taken to be that in the plane of the geomagnetic poles.

Solar Flares

The solar flares that are considered are the same ones considered for the high-altitude orbit, i. e., May 10, 1959, November 12-15, 1960, and February 23, 1956. The free-space spectra of those flares are given at the beginning of Section 3. The manner in which the earth's magnetic field is taken to modify the free-space spectra is discussed in Appendix II.

For the model environment, it is assumed that during the mission, there is an occurrence of one of the three types of flares. Because a cumulative radiobiological tolerance criterion is assumed, the time during the mission when the flare occurs is immaterial.

Cosmic Rays

In order to evaluate the effects of the geomagnetic field on the dose due to the cosmic rays, it is necessary to look at the cosmic ray spectrum in more detail than was done for the high-altitude orbit. A cosmic ray spectrum of the following kind is assumed:

for $4 \leq E \leq 380$ Mev:

$$N_1(E) = 0.514 \times 10^{-4} (1 + 10^{-3} E)^{8.85}$$

for $380 \leq E \leq \infty$ Mev:

(12)

$$N_2(E) = 19.1 \times 10^{-4} (1 + 10^{-3} E)^{-2.4}$$

where

N_1 and N_2 = differential proton flux in particles/(cm²-sec-ster-Mev)

E = proton energy in Mev

The spectrum given by Eq. (12) was based on data given in Fig. 30 of Reference 12, and normalized to agree with the free-space dose of 26 rem/yr that was assumed above.

The effect of the geomagnetic field on the cosmic-ray dose is essentially the same as on the solar-flare dose, except that the free-space cosmic-ray dose is time-independent. The calculation of the cosmic-ray dose for the low-altitude orbit is discussed in Appendix II.

SECTION IV

RADIOBIOLOGICAL TOLERANCE CRITERIA

GENERAL CONSIDERATIONS

The ideal approach to the radiation shielding problem is to stipulate the worst conceivable radiation environment and design a shield behind which the crew experiences no discernible radiobiological effects. Such a shield would be very massive, and, unfortunately, the limited capabilities of boosters of the present and foreseeable future precludes such an approach. Thus weight considerations force us to be a little less conservative in stipulating the environment, and a little more tolerant of minor biological effects. In the previous sections, we postulated a radiation environment that appears reasonable based on present data and slightly, but not overly, conservative. We will now consider what constitutes tolerable radiobiological effects.

The military has traditionally been asked to face higher risks, in performance of their duties involving national security, than have civilians. Extending this reasoning a little further, personnel on military space operations could conceivably be asked to face slightly greater risks than personnel on civilian scientific or exploratory space missions. In the context of military space operations, a risk might also involve the possibility of some biological effects of space radiations that manifest themselves long after the flight is over, e. g. , general life-shortening. The maximum risk that the crew should be asked to face should be a function of the importance of the mission to national security (e. g. , a routine cold-war mission should entail less risk than a general-war mission). Also, in discussing radiation criteria, one should consider not only long-term or chronic effects but also the acute effects that occur during the flight.

For example, while obviously the crew should not sustain a lethal dose, they also should not sustain a temporarily disabling dose that will decrease their efficiency below that necessary to perform their mission. The magnitude of this latter type of dose is a function of the mental and physical difficulty of the task to be performed. Execution of command is a relatively sophisticated task and its performance will not tolerate much degradation in the commander's normal efficiency, thus implying that the commander should only be subjected to a relatively low dose. Another facet of the problem that should be considered is that the effect of a large dose received during the mission might ground the crew for a long period or for life. Since a MOCOP mission could involve very senior, highly trained people, such a situation might be very undesirable.

Taking all the above factors into account, the proposed radiation criteria is based on the philosophy that if the postulated radiation environment does occur, the crew will receive a dose which does not interfere with the performance of their duties but which may result in some minor long-term biological effects.

HIGH-ALTITUDE ORBIT TOLERANCE CRITERION

The most common method of specifying radiobiological tolerance criteria is in terms of cumulative dose (i. e. , the arithmetic sum of all radiation doses received during a mission should not exceed a given amount). For short-duration missions, this is certainly a valid approach. However, for extended duration missions, such as the high-altitude mission under consideration here, this method may not be realistic and may lead to overly pessimistic shielding requirements. For long-duration missions, it may be more realistic to consider the body's ability to recover from sustained radiation damage. A criterion formulated on this basis appears to lead to relaxed shielding requirement--either in

terms of lower shielding weight for a fixed exposure time or extended exposure time for a fixed shielding weight. Application of this criterion to the high-altitude mission is discussed below.

Analytic Formulation

There are experimental indications that biological damage is influenced by radiation rate and interval effects.⁽¹⁵⁾ Rate effect signifies that N rad of radiations received over a year may not be as damaging as N rad received over an hour. Interval effect signifies that two applications of N rad spaced months apart may not be as damaging as two applications of N rad spaced several days apart. These two phenomena seem to imply that there is an ability in biological systems to repair, at least in part, sustained radiation injury. This hypothesis is formulated analytically by Blair^[16] and modified by Davidson^[17] as

$$D_e(t) = D_o \left[f + (1-f) e^{-t/t_c} \right] \quad (13)$$

where

D_e = effective dose

D_o = applied dose

f = nonrecoverable fraction of injury

t_c = characteristic recovery time

The value of f proposed by Blair is 0.10. Schaefer^[18] suggests adding an additional 0.12 to Blair's value to account for the effect of low-energy solar protons which allow no biological recovery. The value of t_c may be taken as 36.1 days in accordance with the recovery half-time value for man of 25 days suggested by Davidson.^[17]

Equation (13) is applicable for finding the residual dose at time t due to an essentially instantaneous dose applied at $t = 0$, and hence may be used for calculating the dose resulting from a solar flare at times much longer than the flare's duration, or the dose resulting from rapid traversal of the Van Allen Belt. Equation (13) can be adapted to obtain the dose due to a prolonged radiation application (such as cosmic rays). If \dot{D} is the variable dose rate, then

$$D_e(t) = \int_0^t \left[f + (1-f) e^{-(t-\tau)/t_c} \right] \dot{D}(\tau) d\tau \quad (14)$$

For a constant rate of application \dot{D}_k (such as will be assumed for cosmic rays), Eq. (14) leads to

$$D_e(t) = \dot{D}_k \left[t f + t_c (1-f) \left(1 - e^{-t/t_c} \right) \right] \quad (15)$$

Quantitative Criteria

Although there is a range of reaction in people subjected to the same acute radiation dose, it is generally held (e.g., Reference 19) that doses in the range 100 to 200 rem produce little or no acute radiation sickness, although chronic effects are known to occur.^[20] Also, data given by Pickering (p. 42 of Reference 15) indicate that doses in this range will have little or no effect on an air-crew's efficiency.

Baum^[21] utilizes the recovery concept formulated by Blair and Davidson, and described in the previous section, in proposing a radiobiological tolerance criterion for astronauts. He suggests that it is permissible for an astronaut to receive four or five 100 rad doses if there is a 120-day recovery period between the exposures. This may be translated as a total of 375 to 400 rad per year of

applied radiation. By the time the astronaut is ready to receive the fifth 100-rad dose, he will have an accumulated residual dose of about 40 rad (see Eq. (13)). Hence, the effective dose at the fifth exposure is $100 + 40 = 140$ rad. It should be noted that Baum expresses his criterion in terms of the absorbed dose unit, the rad, while we have been using the effective biological dose unit, the rem. Since $\text{rem} = \text{rad} \times \text{RBE}$, where $\text{RBE} \geq 1$ for radiations considered herein, we will be conservative by using the numerical values of Baum in terms of rem.

The present study modifies what is essentially Baum's criterion (with slightly more conservative numerical values), and takes into account the slowly applied dose resulting from cosmic rays. The proposed radiation criterion for the long-duration, high-altitude orbit assumes that the effective dose components are defined by Eqs. (13) and (15), and requires that the absorbed dose meets all three of the following conditions.

- (a) The instantaneous applied dose shall not exceed 100 rem.
- (b) The sum of the instantaneous applied and accumulated residual dose shall not exceed 130 rem **at any instant**.
- (c) The total applied dose during a year shall not exceed 350 rem.

It may be noted that this criterion utilizes values for acute and chronic doses that are higher than those usually suggested. Although adherence to this criterion may result in some chronic radiobiological effects, it is felt that this hazard is only commensurate with the other hazards of military space flight.

LOW-ALTITUDE ORBIT TOLERANCE CRITERION

The tours of duty that are assumed for this orbit are in the range of one week to three months. It is assumed that negligible biological recovery occurs in these time periods, so that a cumulative dose criterion is applicable. The cumulative dose limit is taken as 100 rem.

SECTION V

SHIELDING CALCULATIONS

A detailed mathematical description of the radiation transport through a shield material is given in Appendix I. This analysis considers primary protons, secondary protons and neutrons, and bremsstrahlung. The analysis is used to carry out computations on an IBM 7030 STRETCH computer to determine the biological dose behind different amounts of shielding material for the different components of the radiation environment. For the high-altitude orbit, the spectra of the radiation environment components given in Section III are used directly as input to this program. For the low-altitude orbit, the modifying effects of the geomagnetic field on the free-space radiation, as discussed in Appendix II, are fed in as an intermediate step in the computations.

SECTION VI

RESULTS AND DISCUSSION

GENERAL

The results of the shielding computations are shown in the dose curves of Figs. 7 through 10 for the high-altitude orbit and Fig. 11 for the low-altitude orbit. The values for shield thickness (actually in terms of shield weight per unit area) in Figs. 7 through 13 are, of course, the thicknesses of the inner, storm-cellar shielding material that are added to the basic cylindrical shell. To facilitate the calculations, the outer cylindrical shell was replaced by a spherical shell of the same diameter and thickness. Since the outer shell does not contribute materially to the charged particle shielding effectiveness, this

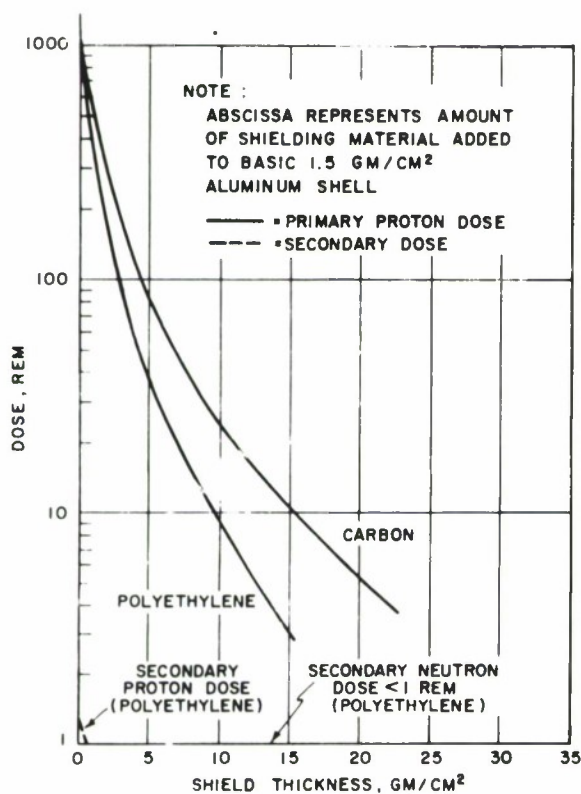


Fig. 7. Dose vs Shield Thickness for
May 10, 1959 (Type A)
Flare (High-Altitude Orbit)

Fig. 8. Dose vs Shield Thickness for November 12-15, 1960 (Type B) Flare Sequence (High-Altitude Orbit)

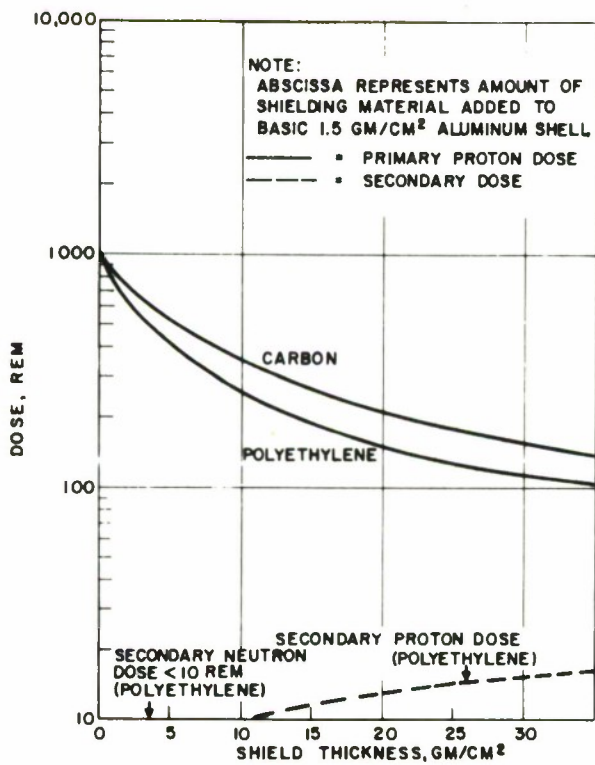
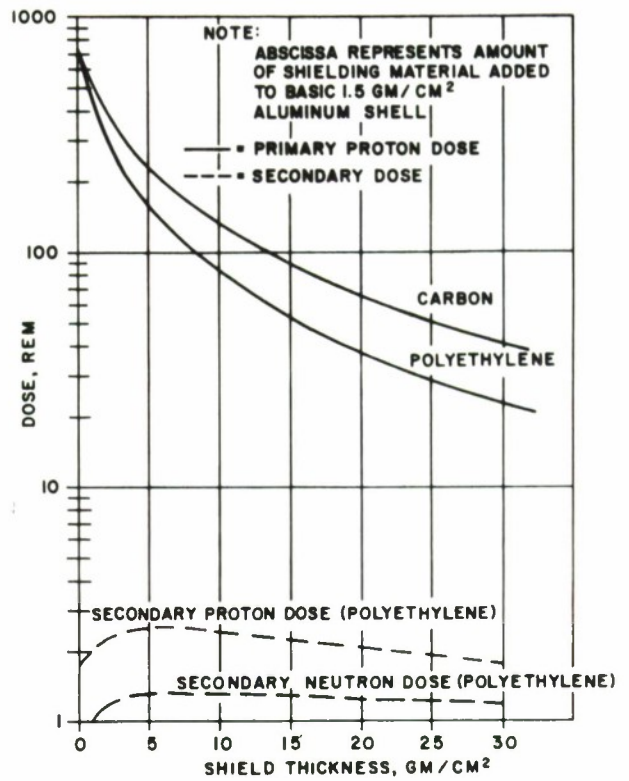


Fig. 9. Dose vs Shield Thickness for February 23, 1956 Flare (High-Altitude Orbit)

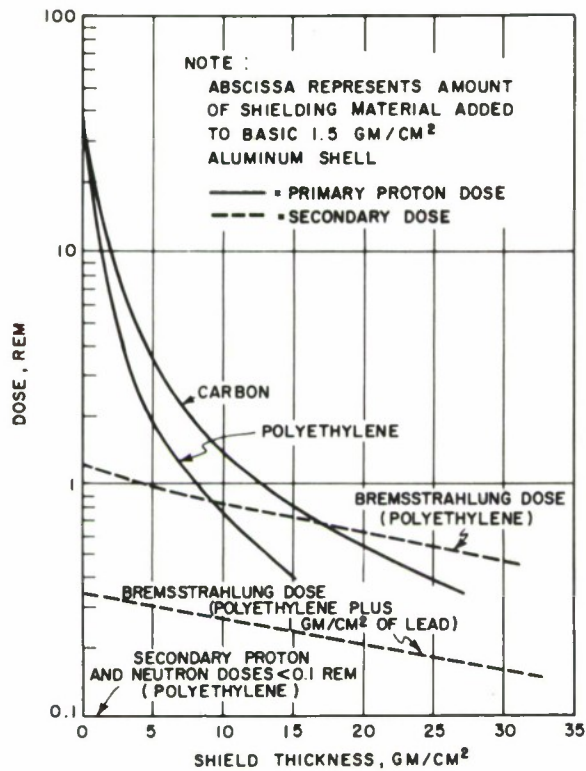


Fig. 10. Dose vs Shield Thickness for Passage Through the Van Allen Belt (High-Altitude Orbit)

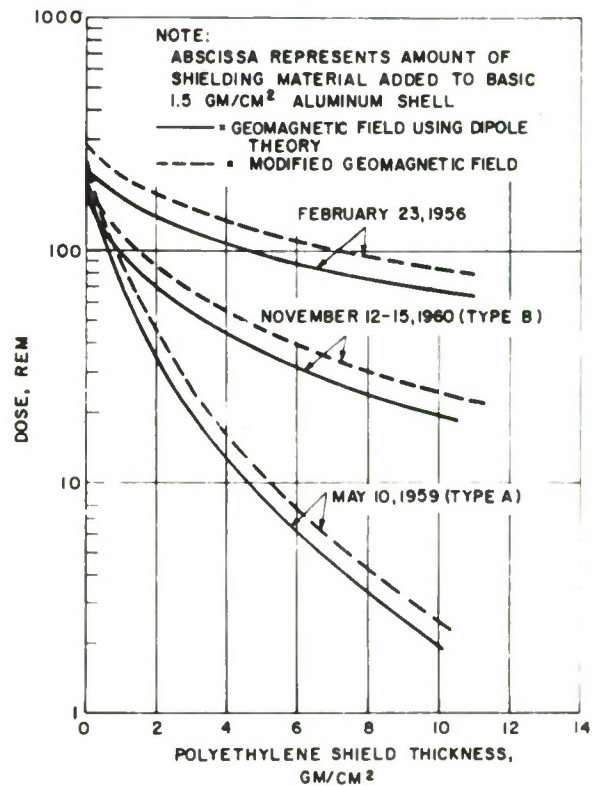


Fig. 11. Primary Proton Dose vs Shield Thickness for three Major Solar Flares (Low-Altitude Polar Orbit)

Fig. 12. Secondary Dose vs Shield Thickness for November 12-15, 1960 Flare Sequence (High-Altitude Orbit)

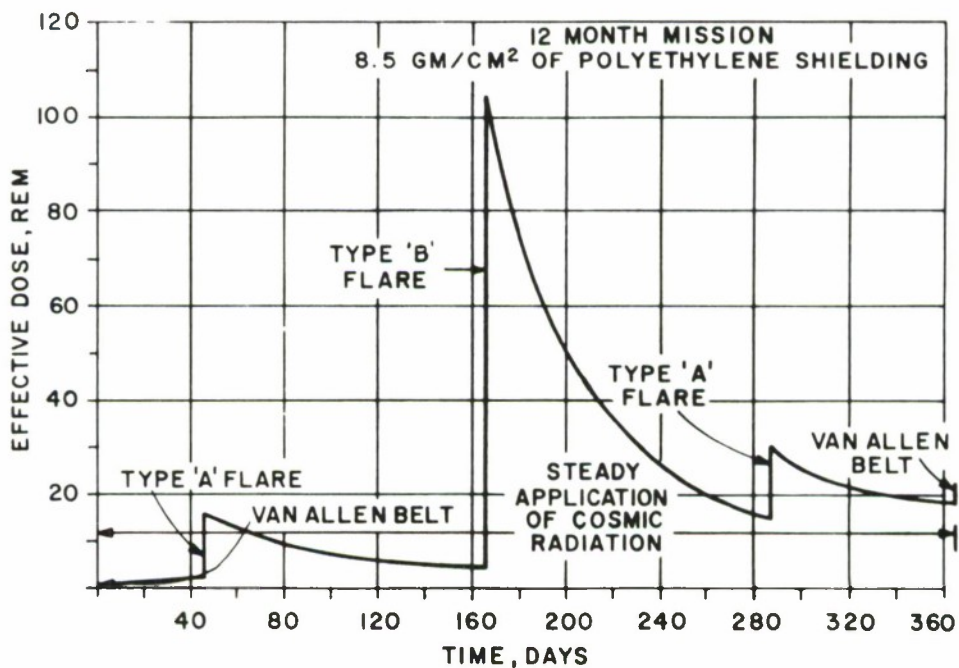
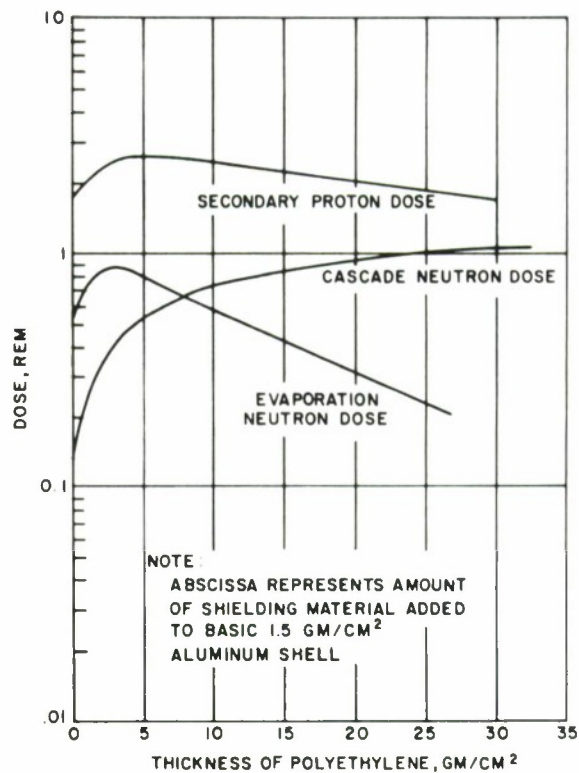


Fig. 13. Effective Dose vs Time (High-Altitude Orbit)

approximation does not significantly affect the results and, further, lies on the conservative side. The aluminum-foamed polyurethane-aluminum sandwich wall of the outer shell was replaced by an equivalent solid aluminum wall of thickness 1.5 gm/cm^2 , since the weight of the foamed polyurethane was a very small part of the total weight of the wall. The biological dose is based on a unit target at the center of the storm cellar. In carrying out the calculations, all protons that penetrate the shield with energies less than 4 Mev are neglected since they can be stopped, for instance, by 45 cm of cabin air at 7 psia or by a thin layer (.015 cm) of body tissue.

The main consideration in the choice of shielding materials was the effectiveness of a given amount of material in attenuating protons. Among the elements, hydrogen is by far the best in this regard, and carbon is second. However, the use of hydrogen was not deemed practical because of storage and containment problems, and the large volume required because of its low density. Consideration was then given to compounds containing large proportions of hydrogen, such as water and polyethylene. The proton range-energy curves for these two materials are almost identical; polyethylene is slightly more effective. This slight edge in effectiveness, plus simpler problems in containment, seem to indicate a superiority of polyethylene over water as a shielding material. Thus, the proton shielding materials used in the high-altitude orbit calculations were carbon and polyethylene (with specific gravity of 1.0), although for all practical purposes, the results of polyethylene are the same as those for water. The calculation results shown in Figs. 7 through 10 indicate the marked superiority of polyethylene over carbon in this application so that only polyethylene was used in the low-altitude orbit calculations.

The dose calculations for the high-altitude orbit considered the contributions made to the total dose by secondary protons and neutrons. As can be seen from Figs. 7 through 10 and Fig. 12, these contributions are small for shield thicknesses in the range of practical interest, and therefore secondary radiations were not considered in the low-altitude orbit calculations.

HIGH-ALTITUDE ORBIT

The dose curves for the various components of the radiation environment are shown in Figs. 7 to 10. Figure 10, which shows the dose received in going through the Van Allen Belt, also illustrates that polyethylene is ineffective in attenuating the secondary, bremsstrahlung radiation caused by the trapped electrons. Note that the addition of 1 gm/cm^2 of lead to the inside of a polyethylene shield reduces the dose by about a factor of 3. However, the rapid passage through the Van Allen Belt for the particular transfer trajectory considered here results in only small amounts of bremsstrahlung, so that the lead is not necessary.

Figures 7 through 10 show that the dose due to secondary protons and neutrons is generally small, and can be neglected with respect to that due to the primary protons. For illustrative purposes, the variation of secondary proton and neutron doses with polyethylene shield thickness for the November 12-15, 1960 flare sequence is shown in Fig. 12. As mentioned previously, the dose due to the electrons was found to be small compared to that due to their bremsstrahlung so that only the latter is shown in Fig. 10.

Figure 9 shows that the dose from the February 23, 1956 flare is substantially larger than that reported elsewhere.^[6, 22] The difference in results for this flare is largely a consequence of differences in the assumed time-variation of the energy spectrum. We have assumed that the flare decays in

time less rapidly than have other authors, [6, 22] and hence our computed total doses are larger. However, our computed initial dose rates do agree with those obtained in References 6 and 22. Since the time-variation of the spectrum is of necessity formulated from measurements at only two times, there are obviously many ways that one can postulate the spectrum's time-variation. In view of this uncertainty, the dose results for this flare, as obtained both here and elsewhere, should be used with caution.

The radiation environment is related to the mission profile and is assumed to be encountered in the following manner. First, the Van Allen radiations are encountered during outward traversal of the belt. Next, the solar flares are encountered with the timewise phasing shown in Section III while the vehicle is on-orbit. Also, while the vehicle is on-orbit, the cosmic radiations are encountered at a constant rate. Finally, the Van Allen radiations are again encountered during inward traversal of the belt. This mission radiation profile may be used in conjunction with the dose curves of Figs 7 through 10, the assumed cosmic-ray dose rate, and the postulated radiobiological tolerance criterion to determine the shielding requirements.

Assuming that the radiation recovery criterion is valid, Eqs. (13) and (15) may be applied to determine the effective dose as a function of time for different thicknesses of a given shield material. Then, by trial-and-error, the minimum thickness that satisfies all conditions of the criterion can be determined. The above procedure was carried out (using $f = 0.10$ and $t = 36.1$ days) and it was found that the minimum thickness of polyethylene for a 12-month mission is 8.5 gm/cm^2 .

The corresponding plot of effective dose versus time is shown in Fig. 13. It is seen that for this case the condition that determines the shield design is

the instantaneous dose from the type-B, November 12-15, 1960 flare sequence. It can also be seen that the sum of the instantaneous and residual dose at any time, even if the type-B flare occurs in the 12th month, is less than 130 rem. Also, the arithmetic sum of the applied doses is well below 350 rem under all conditions. Since the shield is designed by the instantaneous, 100-rem dose, the minimum shield thicknesses for the 6- and 3-month missions are also 8.5 gm/cm² polyethylene. It is interesting to note that if one uses Schaefer's^[18] suggestion for nonrecoverable fraction of 0.22, rather than Blair's^[16] proposed value of 0.10, these results are still valid.

If the model solar-flare environment is modified to include a February 23, 1956 type flare, the shielding requirements are changed dramatically. In this instance, the shield is designed by the instantaneous dose from this flare, and at shielding thicknesses necessary to reduce the dose to 100 rem, the doses from all other sources become almost negligible. Figure 9 shows that the necessary shielding under these conditions is approximately 40 gm/cm² of polyethylene, an increase by a factor of 4.7 over the previous condition. However, as discussed previously, there are uncertainties associated with the data from which the dose curve for this flare was calculated, and the results should be viewed with caution.

LOW-ALTITUDE ORBIT

Dose curves for the three flares under consideration are shown in Fig. 11 for the case of the low-altitude, geomagnetic polar orbit and for both simple and modified geomagnetic cutoffs (see Appendix II). Only the dose due to primary protons is shown, because the shielding calculations for the high-altitude orbit showed the contribution to the total dose due to the secondary radiations to be negligible. Also, calculations were carried out only for a polyethylene shield as the high-altitude orbit case showed this material to be much superior to

carbon for radiation shielding. It should be emphasized that the results associated with the February 23, 1956 flare should be used with caution because of the uncertainties discussed above. Figure 11 shows that use of simple dipole theory gives underestimates of the dose received in polar orbits. The assumed modification of the geomagnetic field due to the magnetic storms accompanying the solar flares is found to increase the doses by 23 to 30 percent.

Comparison of the solar flare dose curves of Fig. 11 with those of Figs. 7, 8, and 9 show the effect of the geomagnetic field in attenuating the proton dose. This attenuation is a function of both the flare's spectrum and the shield thickness. This is illustrated in Fig. 14, where the ratio of geomagnetic-polar-orbit dose (using simple dipole field) to free-space dose is plotted as a function of shield thickness for the three flares of interest. These results show that flares with a "hard" spectrum (a relative abundance of high-energy particles)

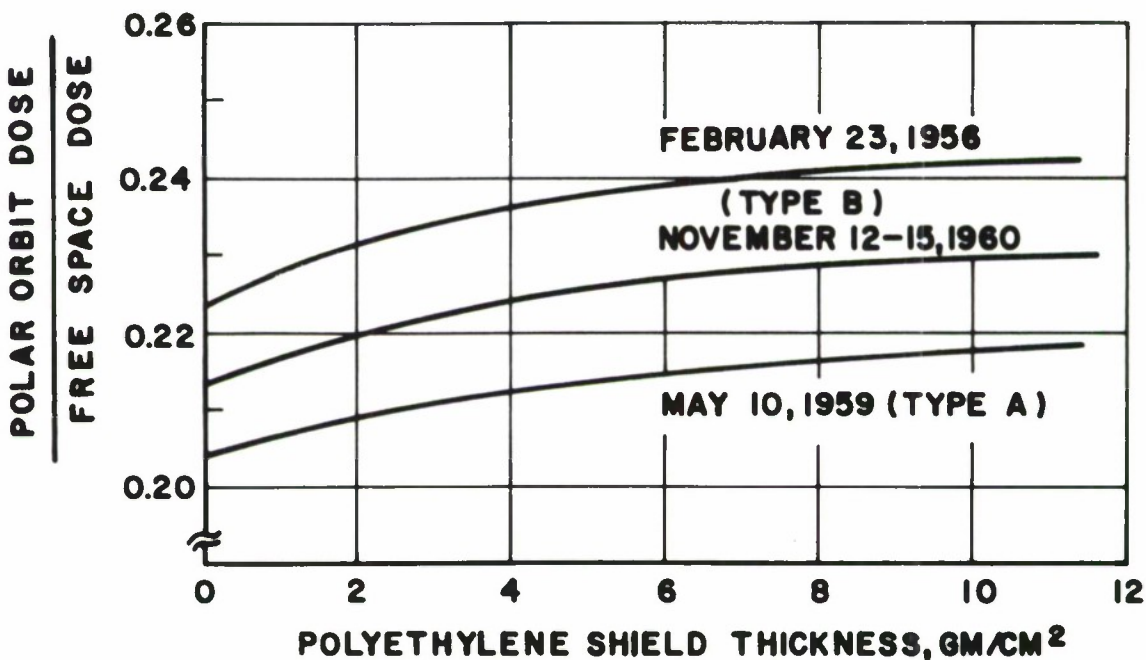


Fig. 14. Ratio of Polar Orbit to Free-Space Dose vs Shield Thickness for 3 Major Solar Flares (Using Simple Dipole Geomagnetic Field)

are attenuated less by the geomagnetic field than are those with a "soft" spectrum. This is a result that would be expected since relative to a soft spectrum a hard spectrum has a higher average energy, and hence the effective geomagnetic cut-off latitude is closer to the equator. This results in the vehicle being irradiated for a longer time, and consequently being subjected to a higher dose per orbit. However, it should be noted that this variation of dose ratio with flare spectrum hardness is not significant, and for a given shield thickness varies by only about 2 percent.

The components of the model environment for this orbit consist of one solar flare and steady cosmic radiations. Calculations show that for the longest mission under consideration for this type of orbit, three months, the cosmic-ray dose is 3 rem. In order to stay within the cumulative dose limit of 100 rem, the solar flare must result in a dose of less than 97 rem. Assuming that a type-A or type-B flare have an equal probability of occurring, it is seen from Fig. 11 that the shielding requirements are dictated by the type-B flare, and that a polyethylene shield thickness of 1.0 gm/cm^2 is required. If the February 23, 1956 flare is considered, the requirement jumps to 5.0 gm/cm^2 .

TOTAL SHIELD WEIGHTS

Up to this point, the radiation shielding requirements have been discussed in terms of shielding thickness (in weight/unit area). However, the quantity of interest to the mission planner and preliminary designer is the total weight of radiation shielding that must be carried. Translation of the shielding requirements from terms of thickness to terms of total shielding weight is straightforward if one stipulates the size and shape of the space that is to be shielded. Basically, there are two choices available to the designer: to shield the entire vehicle; or to shield a minimum size, interior compartment, i. e., a "storm cellar." The former alternative is probably preferable in all respects except a very important

one--weight. For example, the surface area of the vehicle under consideration is 1170 ft^2 ; the weight of shielding to cover the entire vehicle with 8.5 gm/cm^2 of polyethylene (minimum for the high-altitude orbit) is 20,200 lb. While such a weight penalty might be prohibitive for this case, the weight of shielding to cover the entire vehicle with 1.0 gm/cm^2 (minimum for the low-altitude orbit) is 2390 lb, a weight penalty which might be acceptable.

Two factors which play a large role in determining which shielding concept will be used are the total weight that can be placed in orbit, and the fraction of this orbital weight that can be allocated to shielding. The former depends on the capabilities of the boosters that are available at the intended time of launching. The latter depends on the minimum amount of equipment, structure, propulsion, etc., that is necessary to carry out the mission.

The present study is not sufficiently detailed to make a choice between shielding the entire vehicle or using a storm cellar. If the latter course is followed, there remains the problem of choosing a minimum size compartment, which will be influenced by physical and psychological factors, as well as by operational factors such as the tasks that the crew must carry out while within the shelter. It is again beyond the scope of the present study to propose a storm-cellar configuration, but if the crew occupies the shelter once every few months for one or two days, and if the tasks that the crew must perform while within are minimal, then it does not seem unreasonable that a spherical shelter with an inside diameter of 7 ft should suffice for four men. The enclosed volume is then 179 ft^3 and the surface area is 154 ft^2 . The total shield weight to cover this shelter with 8.5 gm/cm^2 and 1.0 gm/cm^2 are 2690 lb and 316 lb, respectively.

It should be noted that for ease of shielding calculations, the vehicle shell was represented by a sphere and the storm cellar was assumed to be an internally concentric sphere. Also, the shielding effects of any internal equipment were not considered. It has been shown^[22, 23] that nonisotropic distribution of shielding material and of equipment can have a very large effect on the internal dose. However, these are refinements which cannot be taken into account in this preliminary study.

Finally, the following are a few suggestions that may be considered for reducing the shielding weight. One possibility for reducing the total weight is through the use of nonhomogeneous thickness shields. These shields can be designed to provide greater protection to the more radiation-sensitive parts of the body such as the head and torso, and less protection to less radiation-sensitive parts such as the arms and legs. Another suggestion is to use the food, water, and waste materials for shielding. Since the consumable stores consist mainly of hydrogenous materials of high shielding efficiency, in amounts sufficient for each man to consume 10 lb/day,^[24] they should be an effective adjunct to the basic shield material. The internal equipment could also be placed to give additional protection to radiation-sensitive parts of the body. It is suggested that complete reliance should not be placed on consumables and internal equipment for radiation protection, as studies have shown that it is difficult in practice to achieve uniform distribution, and that "holes" in the shielding can have effects out of proportion to their size.^[22, 23] In times of acute radiation danger, such as an encounter with a flare that is much larger than expected, a large measure of protection is obtained if the crew huddles together and thus use their group self-shielding ability. Lastly, for large space stations that are proposed for the somewhat distant future, one should investigate the possibility

of using active shielding methods, such as magnetic fields that are generated by super-conducting coils, to deflect rather than stop the charged particles.

Dr. Francis W. French
Dr. Francis W. French

Dr. Kent F. Hansen _{2w7}
Dr. Kent F. Hansen

APPENDIX I

CALCULATION OF RADIATION DOSES

PRIMARY PROTON DOSES

The integral solar flare spectra are characterized by the relation^[5]

$$J (> R, t, \underline{\Omega}) = J_o (t) \exp \left[- \frac{R}{R_o (t)} \right] \quad (16)$$

where $J (> R)$ is the integral directional flux (protons/cm²-sec-ster). R is the proton rigidity (Mv), $\underline{\Omega}$ is a unit vector, and $J_o (t)$ and $R_o (t)$ are reference values for the integral flux and rigidity, The reference values are functions of time.

The particle flux per unit rigidity, $\Phi (R, t, \underline{\Omega})$, is given as

$$\Phi (R, t, \underline{\Omega}) = - \frac{dJ (> R, t, \underline{\Omega})}{dR}$$

whereas the particle flux per unit energy is

$$\begin{aligned} \Phi (E, t, \underline{\Omega}) &= \Phi (R, t, \underline{\Omega}) \frac{dR}{dE} \left(\frac{\text{protons}}{\text{cm}^2 \text{-sec-ster-Mev}} \right) \\ &= \left[\frac{J_o (t)}{R_o (t)} \right] \frac{(E+E_r)}{[(E+E_r)^2 - E_r^2]^{1/2}} \exp \left\{ - \frac{[(E+E_r)^2 - E_r^2]^{1/2}}{R_o (t)} \right\} \quad (17) \end{aligned}$$

The proton flux is assumed to be uniform in the space between the earth's magnetic field and the sun. Further, the flux is assumed isotropic. Consider the spherical shell, an octant of which is shown in Fig. 15.

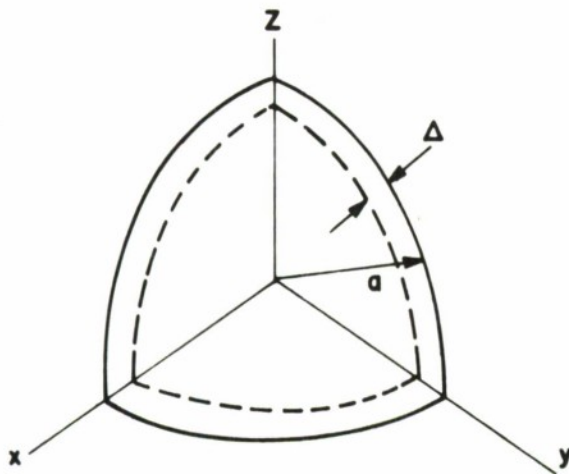


Fig. 15. Shell Geometry

The outer radius of the shell is a (cm), whereas the shell thickness is Δ (gm/cm²).

If a proton with direction vector $\underline{\Omega}'$ is incident upon the shell, then the probability that the proton direction vector crosses an element of area dA at the origin is

$$P(\underline{\Omega}', \underline{\Omega}_r) dA = \delta(\underline{\Omega}' + \underline{\Omega}_r) \frac{dA}{a}$$

where $\underline{\Omega}_r$ is the unit vector from the origin to the outer surface of the shell. The probability that the direction vector crossing a unit area at the origin lies with $d\underline{\Omega}$ of $\underline{\Omega}$ is

$$P(\underline{\Omega}_r, \underline{\Omega}) d\underline{\Omega} = \delta(\underline{\Omega} + \underline{\Omega}_r) d\underline{\Omega}$$

The directional flux of protons at the origin of energy E and direction $\underline{\Omega}$, denoted $\Phi_p(E, t, \underline{\Omega})$, is then the integral over the spherical surface, over all directions, and over all energies of the incident flux,

$$\Phi_p(E, t, \underline{\Omega}) = \int dA \int dE' \int d\underline{\Omega}' \Phi(E', t, \underline{\Omega}') K(E', E, \Delta) * P(\underline{\Omega}_r, \underline{\Omega}) P(\underline{\Omega}', \underline{\Omega}_r)$$

where $K(E', E, \Delta)$ is the probability that a proton of energy E' penetrates a thickness Δ and emerges with energy E . The surface area dA is

$$dA = a^2 d\underline{\Omega}_r$$

hence

$$\Phi_p(E, t, \underline{\Omega}) = \int dE' \Phi(E', t, \underline{\Omega}) K(E', E, \Delta) \quad (18)$$

The function $K(E', E, \Delta)$ is given as

$$K(E', E, \Delta) = 0 \quad \text{if range} < \Delta$$

$$K(E', E, \Delta) = \delta[E - f(E', \Delta)] \quad \text{if range} > \Delta$$

where $f(E', \Delta)$ is found from the range-energy tables for protons. [26] The omnidirectional flux at the origin is

$$\Phi_p(E, t) = 4\pi \Phi_p(E, t, \underline{\Omega})$$

since the source is isotropic.

The dose-rate density in $\frac{\text{rem}}{\text{gm-hr-Mev}}$ at the origin is then

$$\frac{dD_{\text{rem}}}{dt}(E, t) = Q(E) \Phi_p(E, t) \quad (19)$$

where $Q(E)$ is given as

$$Q(E) = 3.6 \times 10^3 \left(\frac{\text{sec}}{\text{hr}}\right) 10^{-2} \left(\frac{\text{rad}}{\text{erg}}\right) 1.6 \times 10^{-6} \left(\frac{\text{erg}}{\text{Mev}}\right) \text{RBE}(E) \left(\frac{\text{rem}}{\text{rad}}\right) \\ g(E) \left(\frac{\text{Mev}}{\frac{\text{gm}}{\text{cm}^2} - \text{proton}}\right) \\ = 5.76 \times 10^{-5} \text{RBE}(E) g(E) \frac{\text{rem}}{\text{gm-hr}} \frac{1}{\text{proton/cm}^2\text{-sec}}$$

Thus $Q(E)$ is the dose rate per unit mass per unit flux. Values of the $\text{RBE}(E)$ and specific energy transfer $g(E)$ versus E are given in Table 3.

All dose rates and doses reported are for a unit volume of tissue (H_2O) located at the origin. The low-energy limit for protons was taken as 4 Mev, since protons of lower energy would be stopped by the air with the capsule.

Table 3

Dose Rate Per Unit Mass Per Unit Flux

(From References 6 and 27)

<u>E (Mev)</u>	<u>RBE (E)</u>	<u>rem</u> <u>rad</u>	<u>g (E)</u>	<u>Mev</u> <u>gm/cm²-proton</u>	<u>Q (E)</u>	<u>rem</u> <u>gm-hr-flux</u>
4	2.6		100			1.5×10^{-2}
6	2.1		72			$.87 \times 10^{-2}$
8	1.7		56			$.55 \times 10^{-2}$
10	1.5		47			$.41 \times 10^{-2}$
15	1.3		35			$.26 \times 10^{-2}$
20	1.2		27			$.19 \times 10^{-2}$
30	1.0		20			$.12 \times 10^{-2}$
40	1.0		16			$.92 \times 10^{-3}$
60	1.0		13			$.75 \times 10^{-3}$
100	1.0		7			$.40 \times 10^{-3}$
140	1.0		6			$.35 \times 10^{-3}$
200	1.0		5			$.29 \times 10^{-3}$
250	1.0		4			$.23 \times 10^{-3}$
400	1.0		3.5			$.20 \times 10^{-3}$
600	1.0		3.0			$.17 \times 10^{-3}$
1000	1.0		2.5			$.14 \times 10^{-3}$
2000	1.0		2.5			$.14 \times 10^{-3}$
5000	1.0		3.0			$.17 \times 10^{-3}$
5100	1.0		3.0			$.17 \times 10^{-3}$

The dose rate is

$$\frac{dD_{\text{rem}}(t)}{dt} = \int dE Q(E) \Phi_p(E, t) \quad (20)$$

while the dose is

$$D_{\text{rem}} = \int dt \left[\frac{dD_{\text{rem}}(t)}{dt} \right] \quad (21)$$

The numerical evaluation of the dose was performed as follows: a discrete set of energies E_k was selected; the flux density was computed by use of the range-energy tables and Eq. (17); the dose rate density was evaluated from Eq. (19); and the dose rate was computed by Eq. (20), using the trapezoidal rule. Similarly, the dose was computed by Eq. (21), again using the trapezoidal rule.

SECONDARY PROTON DOSES

The directional flux of proton secondaries at the origin is denoted

$$\Phi_s(E, t, \underline{\Omega}) \frac{\text{protons}}{\text{cm}^2 \text{-sec-ster-Mev}}$$

An integral expression for the secondary proton flux is

$$\Phi_s(E, t, \underline{\Omega}) = \int d\underline{r} \int dE' \int d\underline{\Omega}' \left\{ T_s(\underline{r}, E', \underline{\Omega}', E, \underline{\Omega}) \int dE'' \int d\underline{\Omega}'' \left[K_s(E'', \underline{\Omega}''; E', \underline{\Omega}') \Sigma_p(\underline{r}, E'') \Phi(\underline{r}, E'', \underline{\Omega}'') \right] \right\} \quad (22)$$

where the term in square brackets represents the birth rate density of secondaries and the term in braces represents the transmission function of secondary particles.

In particular

$T_s(\underline{r}, E', \underline{\Omega}'; E, \underline{\Omega})$ = probability that a proton at position \underline{r} with energy E' and direction $\underline{\Omega}'$ will cross a unit area at the origin with energy E and direction $\underline{\Omega} \left(\frac{1}{\text{Mev-cm}^2\text{-ster}} \right)$

$K_s(E'', \underline{\Omega}'; E', \underline{\Omega}')$ = probability that a collision by a proton of energy E'' and direction $\underline{\Omega}''$ will produce a secondary proton with energy E' and direction $\underline{\Omega}' \left(\frac{\text{protons}}{\text{Mev-ster}} \right)$

$\Sigma_p(\underline{r}, E'')$ = macroscopic proton inelastic collision cross-section (cm^{-1}).

The function K_s represents both cascade and evaporation processes. The evaporation protons are of sufficiently low energy ($E' < 25$ Mev) that few penetrate the shield and may be ignored. The cascade protons are strongly directed in a forward cone relative to the primary proton. For simplicity, all cascade protons are assumed monodirectional and equal to the primary proton direction. This approximation overestimates the secondary dose. However, ignoring contributions from secondaries produced by primaries of different directions tends to compensate for the approximation. We then have

$$K_s(E'', \underline{\Omega}'', E', \underline{\Omega}') = \bar{n}_s(E'', E') \delta(\underline{\Omega}'' - \underline{\Omega}')$$

where $\bar{n}_s(E'', E')$ is the number spectrum of cascade protons produced by primaries of energy E'' . The cascade proton spectrum is simplified by assuming an average energy for the secondaries. An empirical relation

$$\bar{n}_s(E'', E') = \bar{n}_s(E'') \delta\left(E'' - \frac{E'}{.445}\right)$$

is assumed. Thus we have

$$\begin{aligned} & \int dE'' \int d\underline{\Omega}'' K_s(E'', \underline{\Omega}''; E', \underline{\Omega}') \Sigma_p(\underline{r}, E'') \Phi(\underline{r}, E'', \underline{\Omega}'') \\ &= \bar{n}_s\left(\frac{E'}{.445}\right) \Sigma_p\left(\underline{r}, \frac{E'}{.445}\right) \Phi\left(\underline{r}, \frac{E'}{.445}, \underline{\Omega}'\right) \\ & \quad \left(\frac{\text{protons}}{\text{cm}^3 \text{-sec-ster-Mev}}\right) \end{aligned}$$

The transfer probability T_s is easily derived from previous results. In particular

$$T_s(\underline{r}, E', \underline{\Omega}''; E, \underline{\Omega}) = K[E', E, \Delta(\underline{r})] \delta(\underline{\Omega}' + \underline{\Omega}_r) \frac{1}{r} \delta(\underline{\Omega}_r + \underline{\Omega})$$

Hence,

$$\begin{aligned} \Phi_s(E, t, \underline{\Omega}) &= \int r^2 dr \int d\underline{\Omega}_r \int dE' \int d\underline{\Omega}' \frac{K[E', E, \Delta(\underline{r})]}{r^2} \delta(\underline{\Omega}' + \underline{\Omega}_r) \\ & \quad * \delta(\underline{\Omega}_r + \underline{\Omega}) \bar{n}_s\left(\frac{E'}{.445}\right) \Sigma_p\left(\underline{r}, \frac{E'}{.445}\right) \Phi\left(\underline{r}, \frac{E'}{.445}, \underline{\Omega}'\right) \quad (23) \\ &= \int dE' \int dr K[E', E, \Delta(\underline{r})] \bar{n}_s\left(\frac{E'}{.445}\right) \Sigma_p\left(\underline{r}, \frac{E'}{.445}\right) \Phi\left(\underline{r}, \frac{E'}{.445}, \underline{\Omega}\right) \end{aligned}$$

The omnidirectional secondary proton flux at the origin is

$$\Phi_s(E, t) = 4\pi \Phi_s(E, t, \underline{\Omega})$$

The numerical integration of Eq. (23) is performed as follows: for any energy E , the various values of E' as a function of r (i. e., $\Delta(r)$) are found from the range-energy tables; the corresponding primary energy, $\frac{E'}{.445}$, is computed and used to find $\bar{n}_s \left(\frac{E'}{.445} \right)$ and $\Sigma_p \left(r, \frac{E'}{.445} \right)$; the range-energy tables are used to find the primary proton energy outside the shell; and hence the primary flux is evaluated from Eq. (17). Having found the secondary flux at the origin, the dose rate and dose is computed as before.

The data used for the calculations is given in the following tables.

Table 4

Number and Energy of Cascade Protons^[28]

<u>Primary Proton Energy (Mev)</u>	<u>Mean No. of Cascade Protons</u>	<u>Average Cascade Proton Energy (Mev)</u>
50	.56	18
100	.66	36
200	.86	74
400	.95	148
1000	1.12	445
2000	1.50	890

Table 5

Proton Inelastic Cross-Sections^[28]

<u>Proton Energy (Mev)</u>	<u>Inelastic Cross-Section (mb)</u>
25	450
50	350
100	250
200	250
400	250
1000	250

SECONDARY NEUTRON DOSES

The directional flux of neutron secondaries at the origin is denoted

$$\Phi_n(E, t, \underline{\Omega}) \left(\frac{\text{neutrons}}{\text{cm}^2 \text{-sec-ster-Mev}} \right).$$

The integral expression, Eq. (22), holds for neutrons with the appropriate modification of the kernels T and K .

For cascade neutrons we again assume forward scatter and a primary-secondary energy correlation. In particular we assume

$$K_{nc}(E'', \underline{\Omega}''; E', \underline{\Omega}') = \bar{n}_{nc} \left(\frac{E'}{.30} \right) \delta \left(E'' - \frac{E'}{.30} \right) \delta (\underline{\Omega}'' - \underline{\Omega}') \quad (24)$$

where the subscript nc denotes cascade neutrons.

The transmission function for neutrons is given by

$$T_n(\underline{r}, E', \underline{\Omega}'; E, \underline{\Omega}) = e^{-\tau(\underline{r}, E) \frac{\delta(\underline{\Omega}' + \underline{\Omega}_r)}{r^2}} \delta(\underline{\Omega}_r + \underline{\Omega}) \delta(E' - E) \quad (25)$$

where $\tau(\underline{r}, E)$ is the optical depth of the material for neutrons. Since any collision changes the neutron direction and energy, the functions $e^{-\tau(\underline{r}, E)}$ and $\delta(E' - E)$ appear. Thus we are computing the unscattered neutron flux at the origin. The contribution of scattered neutrons is very small since the mean free path of the cascade neutrons is considerably larger than Δ .

The flux of cascade neutrons at the origin is then

$$\Phi_{nc}(E, t, \underline{\Omega}) = \int dr e^{-\tau(r, E)} \Sigma_p \left(r, \frac{E'}{.30} \right) \overline{n_{nc}} \left(\frac{E'}{.30} \right) \Phi_p \left(r, \frac{E'}{.30}, \underline{\Omega} \right) \quad (26)$$

The numerical integration of Eq. (26) is performed in a manner analogous to the cascade protons.

Evaporation neutrons are computationally more complex since the evaporation neutrons are isotropically emitted from the nucleus. The birth-rate density of evaporation neutrons of energy E' and direction $\underline{\Omega}'$ is then

$$\int dE'' \overline{n_{ne}}(E'', E') \frac{\Sigma_p(r, E'')}{4\pi} \int d\underline{\Omega}'' \Phi(r, E'', \underline{\Omega}''). \quad (27)$$

The transmission function for the evaporation neutrons is the same as for cascade neutrons and given by Eq. (25). The directional flux of evaporation neutrons at the origin is then

$$\Phi_{ne}(E, t, \underline{\Omega}) = \int dr \frac{e^{-\tau(r, E)}}{4\pi} \int dE'' \overline{n_{ne}}(E'', E) \Sigma_p(r, E'') * \int d\underline{\Omega}'' \Phi(r, E'', \underline{\Omega}'') \quad (28)$$

The evaluation of the angular integral in Eq. (28) is performed by a simplified quadrature,

$$\int d\underline{\Omega}'' \Phi(r, E'', \underline{\Omega}'') = 2\pi \int_{-1}^1 d\mu \Phi(r, E'', \mu) \quad (29)$$

where μ is the cosine of the angle between the proton direction and the radius vector. Associated with any value of μ there is a fixed shield thickness. The shield thickness and range-energy tables are used in conjunction with Eq. (17) to evaluate the directional flux. Equation (29) is integrated numerically to find the omnidirectional flux of protons of energy E'' at position r .

The collision cross-section is the same as that given in Table 5.

The function $\overline{n}_{ne}(E'', E)$ is written as

$$\overline{n}_{ne}(E'', E) = \overline{n}_{ne}(E'') p(E'', E)$$

with $\overline{n}_{ne}(E'')$ the mean number density of evaporation neutrons, which is tabulated in Table 6, and $p(E'', E)$ the energy distribution function for evaporation neutrons. The evaporation neutron energy spectrum is given as^[28]

$$p(E'', E) = \frac{E}{\theta^2} \exp\left(-\frac{E}{\theta}\right)$$

with θ the nuclear temperature which is correlated with the incident energy as

$$\theta^2 = \frac{57}{A} (E'')^{.322}$$

with A the atomic weight.

The calculation proceeds in a manner similar to the cascade neutrons.

Table 6

Mean Number of Cascade and Evaporation Neutrons per
Inelastic Collision^[28]

<u>Primary Proton Energy (Mev)</u>	<u>Mean No. of Cascade Neutrons</u>	<u>Mean No. of Evaporation Neutrons</u>
50	.30	.70
100	.40	.70
200	.60	.70
400	.80	.70
1000	1.00	.80
2000	1.20	1.00

The neutron dose in rem per unit neutron flux as a function of energy is listed in Table 7.

Table 7

Neutron Doses per Unit Flux as a Function of Neutron
Energy^[29]

<u>Neutron Energy (Mev)</u>	<u>Dose (Rem/hr-flux x 10³)</u>
12	.270
10	.270
8	.260
6	.230
4	.195
2	.148
1	.136
.5	.083
.1	.03

ELECTRON DOSES

The Van Allen electrons have energies ranging up to ~ 3 Mev which is sufficiently low that all electrons will be stopped in the outer shell of the capsule. The bremsstrahlung is the only radiation hazard from the electrons.

The electron omnidirectional flux is denoted

$$\Phi_e (E, t) \left(\frac{\text{electrons}}{\text{cm}^2 \text{-sec-mev}} \right).$$

Only 1/2 of the flux is incident upon the spacecraft surface and from the isotropy of the distribution, the electron penetration will vary from 0 to the maximum range. Detailed electron trajectories are very complicated and the simplifying assumptions are made that all electrons stop at a fixed distance within the shield, and further, that the bremsstrahlung is produced at the point of stopping.

The angular distribution of electrons within the shield will approach isotropy within a short travel distance due to elastic collisions. It is therefore a good approximation to assume the bremsstrahlung is isotropically distributed. The omnidirectional photon flux is denoted

$$\Phi (h\nu, t) \left(\frac{\text{Photons}}{\text{cm}^2 \text{-sec-Mev}} \right)$$

For an electron of energy E , stopping in a material of atomic number z , the bremsstrahlung intensity of energy $h\nu$, is given as^[30]

$$I (h\nu) = 2zk (E-h\nu) \text{ per electron}$$

with $I (h\nu) =$ number of photons times the photon energy

Thus

$$\begin{aligned} \Phi(h\nu, t) &= \frac{I(h\nu)}{h\nu} * \Phi_e(E, t) \quad 0 \leq h\nu \leq E \\ &= \frac{2kz}{h\nu} \int_0^{E_{\max}} (E-h\nu) \Phi_e(E, t) dE \quad \frac{\text{photons}}{\text{cm}^2 \text{-sec-Mev}} \quad (30) \end{aligned}$$

The source surface is located as in Fig. 16.

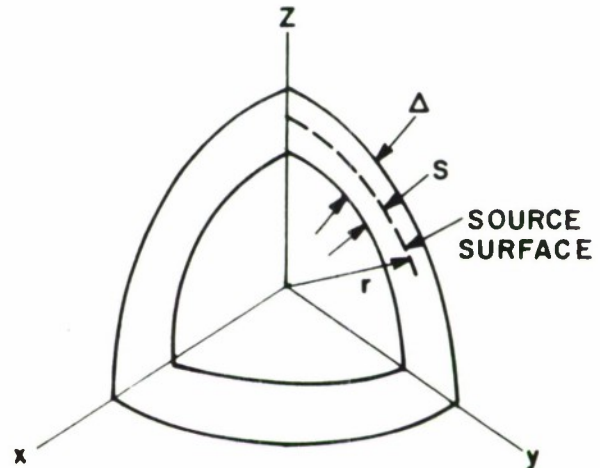


Fig. 16 Bremsstrahlung Source Surface

The total shell thickness is $\Delta \frac{\text{gms}}{\text{cm}^2}$. The thickness of material from the source surface to the inner edge is $s \frac{\text{gms}}{\text{cm}^2}$. The radius to the source surface is r (cm).

The probability that a photon emitted from the source surface will cross a unit area at the origin is $1/4 \pi r^2$. The total emitting surface area is $4\pi r^2$, hence the photon flux at the origin is

$$\Phi_0(h\nu, t) = e^{-\tau(h\nu, s)} \Phi(h\nu, t),$$

with $\tau(h\nu, t)$ the optical path for photons of energy $h\nu$. The photon-dose-rate density at the origin is the intensity at the origin times the mass absorption coefficient for H_2O .

$$\frac{dD(h\nu, t)}{dt} = e^{-\tau(h\nu, s)} \Phi(h\nu, t) h\nu \frac{\mu_a}{\rho} \frac{\text{Mev}}{\text{sec-gm-Mev}}$$

The dose rate density in $\frac{\text{rem}}{\text{hr-Mev}}$ is

$$\begin{aligned} \frac{dD_{\text{rem}}(h\nu, t)}{dt} &= R(h\nu) e^{-\tau(h\nu, s)} \Phi(h\nu, t) h\nu \frac{\mu_a(h\nu)}{\rho} \\ &= R(h\nu) e^{-\tau(h\nu, s)} \frac{\mu_a(h\nu)}{\rho} (h\nu) \text{Zkt} \int_0^E (E-h\nu) \Phi(E, t) dE \quad (31) \end{aligned}$$

The dose rate and dose are computed by integrating Eq. (31) over energy and time.

The bremsstrahlung dose calculated from Eq. (31) represents the dose from primary photons, i. e., uncollided photons. The build-up of secondary and higher order photons will be a few percent at best and is ignored in comparison with other uncertainties.

APPENDIX II

POLAR ORBIT DOSES

Below the earth's geomagnetic field the proton spectrum is depleted due to deflection by the geomagnetic field. The cutoff energy is a function of geomagnetic latitude. For vertically directed protons the cutoff rigidity, P^* , is approximated as^[31]

$$P^* = P_0 \cos^4 \theta \quad (32)$$

with θ the geomagnetic latitude and $P_0 = 14.9 \frac{\text{Bev}}{c}$, where c is the speed of light. The relativistic relation between the cutoff rigidities and cutoff energy E^* is then

$$E^* (\theta) = \sqrt{P_0^2 c^2 \cos^8 \theta + E_r^2} - E_r \quad (33)$$

with E_r ($\equiv .938$ Bev) the proton rest energy.

It should be noted that Eq. (32) is derived by assuming that the geomagnetic field is a simple dipole which is an adequate representation in times of low solar activity. However, it has been found that the magnetic storms that accompany solar flares act to decrease the cutoff rigidity at a given latitude from that predicted by simple dipole theory. This results in an effective shrinking of the magnetically shielded region around the earth so that dose calculations made on the basis of simple dipole theory give results that are larger than the actual. An average correction for the modified geomagnetic field has been suggested by Webber^[32] and is shown below in Fig. (17) as a plot of effective geomagnetic

latitude versus actual geomagnetic latitude, for use with Eq. (32).

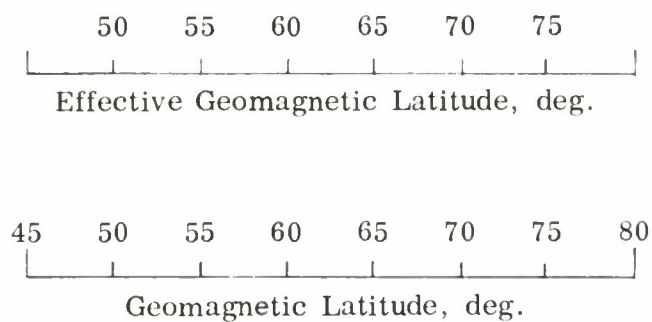


Fig. 17 Modification of Geomagnetic Field During Solar Flare [32]

At any time t , a vehicle in polar orbit will be shielded by the earth's field. Let the differential proton directional flux be denoted as

$$\varphi(E, \underline{\Omega}, t) \frac{\text{protons}}{\text{cm}^2 \text{-sec-ster-Mev}}$$

The instantaneous dose rate is, at time t ,

$$\frac{dD(t)}{dt} = 4\pi \int_{E^*(t)}^{\infty} dE K(E) \varphi(E, \underline{\Omega}, t) \frac{\text{rem}}{\text{sec}} \quad (34)$$

with $K(E)$ the flux-to-dose conversion factor.

The integral (Eq. 34) may be divided into two parts, dose due to particles at or below the maximum cutoff energy, say E_m^* , and dose due to particles above the maximum cutoff. Hence,

$$\frac{dD(t)}{dt} = 4\pi \int_{E^*(t)}^{E_m^*} dE K(E) \varphi(E, \underline{\Omega}, t) + 4\pi \int_{E_m^*}^{\infty} dE K(E) \varphi(E, \underline{\Omega}, t) \frac{1 \text{ cm}}{\text{sec}} \quad (35)$$

For cosmic rays, the proton flux in free space is assumed constant with time, while for solar flares it varies over the life of the flare. Thus, the computation of the dose due to solar flares involves a timewise integration over the life of the flare. The discussion presented herein of dose calculation in polar orbits is in terms of solar flare dose; the application of the method for calculation of cosmic ray dose should be obvious.

For the low-altitude circular orbits being considered, the vehicle's angular velocity is constant and equal to 2π radians in about 90 minutes. It is assumed that the geomagnetic field is symmetric about planes containing the geomagnetic poles and the geomagnetic equator so that for a constant flux, only a quarter orbit need be considered. The vehicle traverses a quarter orbit in about 22.5 minutes. The small changes in the solar flare flux during this interval are neglected and the flux is taken as constant during at least one quarter orbit. Therefore an average dose rate during a quarter orbit is computed as

$$\left(\frac{dD(t)}{dt} \right)_{\text{avg.}} = 4\pi \left(\frac{2}{\pi} \right) \int_0^{\pi/2} d\theta \int_{E^*(\theta)}^{E_m^*} dE K(E) \varphi(E, \underline{\Omega}, t) + 4\pi \int_{E_m^*}^{\infty} dE K(E) \varphi(E, \underline{\Omega}, t) \quad (36)$$

The numerical integration of Eq. (36) is carried out as follows: A discrete set of J energies E_j are chosen. For $E_j \leq E_m^*$ the corresponding θ , (from Eq. 33)) is obtained. Let $E_{j_m} \equiv E_m^*$ so that $\theta_{j_m} = 0^0$. For energies above cutoff, the contribution to the dose rate is obtained as

$$I_J \equiv \int_{E_m^*}^{\infty} dE K(E) \varphi(E, \underline{\Omega}, t) \approx \sum_{j=j_m}^J \Delta E_j \omega_j K(E_j) \varphi(E_j, \underline{\Omega}, t) \quad (37)$$

with ω_j the weighting coefficients.

For energies below cutoff we have, (dropping the star superscript)

$$\begin{aligned} \frac{2}{\pi} \int_0^{\pi/2} d\theta \int_{E(\theta)}^{E_m} dE K(E) \varphi(E, \underline{\Omega}, t) &= \frac{1}{90} \left[\int_{\theta_{j_m}}^{\theta_{j_m}^{-1}} d\theta \int_{E(\bar{\theta}_{j_m})}^{E_m} dE K(E) \varphi(E, \underline{\Omega}, t) + \dots \right. \\ &\left. + \int_{\theta_j}^{\theta_{j-1}} d\theta \int_{E(\bar{\theta}_j)}^{E_m} dE K(E) \varphi(E, \underline{\Omega}, t) + \dots + \int_{\theta_2}^{\theta_1 = \pi/2} d\theta \int_{E(\bar{\theta}_2)}^{E_m} dE K(E) \varphi(E, \underline{\Omega}, t) \right] \quad (38) \end{aligned}$$

where

$$\int_{E(\bar{\theta}_j)}^{E_m} dE K(E) \varphi(E, \underline{\Omega}, t) \approx \frac{1}{2} \left[\int_{E(\theta_j)}^{E_m} () + \int_{E(\theta_{j-1})}^{E_m} () \right]$$

Define

$$I_j = \int_{E(\bar{\theta}_j)}^{E(\theta_{j+1})} dE K(E) \varphi(E, \underline{\Omega}, t) \quad (j = 1, 2, \dots, j_m - 1) \quad (39)$$

Then

$$\begin{aligned} \int_{E(\theta_j)}^{E_m} () &= \int_{E(\theta_j)}^{E(\theta_{j+1})} () + \int_{E(\theta_{j+1})}^{E(\theta_{j+2})} () + \dots + \int_{E(\theta_{j_m-1})}^{E_m} () \\ &= I_j + I_{j+1} + \dots + I_{j_m-1} \end{aligned} \quad (40)$$

Therefore

$$\begin{aligned} \int_{E(\bar{\theta}_j)}^{E_m} dE K(E) \varphi(E, \underline{\Omega}, t) &\approx \frac{1}{2} \left[(I_j + I_{j+1} + \dots + I_{j_m-1}) + (I_{j-1} + I_j + \dots + I_{j_m-1}) \right] \\ &= \frac{I_{j-1}}{2} + I_j + \dots + I_{j_m-1}, \end{aligned} \quad (41)$$

Define

$$S_{j_m-1} = \left(\frac{\theta_{j_m-1} - \theta_{j_m}}{90} \right) \frac{I_{j_m-1}}{2}$$

$$S_{j_m-2} = \left(\frac{\theta_{j_m-2} - \theta_{j_m-1}}{90} \right) \left(\frac{I_{j_m-2}}{2} + I_{j_m-1} \right) \quad (42)$$

⋮

$$S_j = \left(\frac{\theta_j - \theta_{j+1}}{90} \right) \left(\frac{I_j}{2} + I_{j+1} \cdots + I_{j_m-1} \right)$$

Then

$$\left(\frac{dD(t)}{dt} \right)_{\text{avg.}} = 4\pi \left(\sum_{j=1}^{j_m-1} S_j + I_J \right) \quad (43)$$

Calculation of the total dose is then performed by numerical integration of $\left(\frac{dD(t)}{dt} \right)_{\text{avg.}}$ over t by any convenient quadrature.

REFERENCES

1. Power, T. S. , "Military Aspects of Manned Space Flight," 2nd Manned Space Flight Meeting, Dallas, Texas, April 22-24, 1963, pp. 4-8.
2. French, F. W. , and L. J. Mente, "Vulnerability of A Manned Orbital Command Post to Nuclear Bursts," 8th Symposium on Ballistic Missile and Space Technology, San Diego, California, October 16-18, 1963, (SRD)
3. Webber, W. R. , and P. S. Freier, "An Evaluation of the Radiation Hazard Due to Solar Cosmic Rays," Proc. of Symposium on the Protection Against Radiation Hazards in Space, Gatlinburg, Tennessee, November 5-7, 1962, pp. 12-32.
4. Malitson, H. H. , and W. R. Webber, "A Summary of Solar Cosmic Ray Events," Solar Proton Manual, NASA TR R-169, December 1963.
5. Freier, P. S. , and W. R. Webber, "Experimental Rigidity Spectrums and Solar Flare Cosmic Rays," Journal of Geophysical Research, vol, 68, no. 6, March 15, 1963, pp. 1605-1629.
6. Foelsche, T. , "Current Estimates of Radiation Doses in Space," NASA TN D-1267, July 1962.
7. "Program 461 Reliability, Materials Research and Application, Penetrating Radiation Investigation," Lockheed Missiles and Space Company, Report No. LMSC-A324750, 17 June 1963.
8. Smith, R. V. , et al, "Proton Flux Measurements from Satellites 1961 Sigam-1, 1961 Alpha-Delta-1, and 1962 Kappa-1 Near the Peak of the Inner Van Allen Belt", Lockheed Missiles and Space Company, Report No. LMSC 2-08-62-2, June 1962.
9. Russak, S. L. , "Radiation Dosages from Electrons and Bremsstrahlung in the Van Allen Belts," Proc. of Symposium on the Protection Against Radiation Hazards in Space, Gatlinburg, Tennessee, November 5-7, 1962, pp. 760-772.

10. Pizzella, G., Laughlin, C. D., and B. J. O'Brien, "Note on the Electron Energy Spectrums in the Inner Van Allen Belt," Journal of Geophysical Research, vol. 67, no. 9, September 1962, p. 3281.
11. Tamplin, A. R., and H. K. Fisher, "Galactic Cosmic Radiation and Manned Space Flight," Rand Corporation, Memorandum RM-3043-PR, December 1962.
12. Milford, S. N., "Cosmic Ray Hazards in the Solar System," AIAA Aerospace Sciences Meeting, New York, N. Y., January 22-24, 1964, Preprint No. 65-66.
13. Tobias, C. A., "Radiation Hazards in High Altitude Aviation," WADC Rechnical Report 52-119, May 1952.
14. Saylor, W. P., Winer, D. E., Eiwen, C. J., and A. W. Carriker, "Space Radiation Guide," Aerospace Medical Division Report AMRL-TDR-62-86, August 1962.
15. Jacobs, G. J., ed., Proceedings of Conference on Radiation Problems in Manned Space Flight, Washington, D. C., June 21, 1960, NASA TN D-588, December 1960.
16. Blair, H. A., "A Formulation of the Injury, Life Span, Dose Relations for Ionizing Radiation," University of Rochester Report UR-206, May 13, 1952.
17. Davidson, H. O., Biological Effects of Whole-Body Gamma Radiation on Human Beings, Johns Hopkins Press, Baltimore, Md., 1957.
18. Schaefer, H. J., "Radiation Tolerance Criteria in Space Operations," ARS Journal, vol. 32, no. 5, May 1962, pp. 771-773.
19. Glasstone, S., ed. The Effects of Nuclear Weapons, Revised Edition, U. S. Government Printing Office, p. 592, April 1962.
20. Nuclear Radiation Guide, AFSC Aerospace Medical Division Report MRL-TDR-62-61, November 1962, p. 62.
21. Baum, S. J., "Recommended Ionizing Radiation Exposures for Early Exploratory Space Missions," Aerospace Medicine, vol. 33, no. 10 October 1962, pp. 1182-1186.

22. Beck, A. J. , and E. L. Divita, "Evaluation of Radiation Doses Received Within A Typical Spacecraft," ARS Journal, vol. 32, no. 11 November 1962, pp. 1668-1676.
23. Russak, S. F. , "Radiation Shielding Considerations in Manned Spacecraft Design," Journal of Spacecraft and Rockets, vol. 1, no. 3, May-June 1964, pp. 310-316.
24. Keller, W. J. , "Long Range NASA Shielding Requirements," Proc. of Symposium on the Protection Against Radiation Hazards in Space, Gatlinburg, Tennessee, November 5-7, 1962, pp. 662-681.
25. Wallner, L. E. , and H. R. Kaufman, "Radiation Shielding for Manned Space Flight," NASA TN D-681, July 1961.
26. Atkinson, J. H. , and B. H. Willis, "High Energy Particle Data," U. of California Radiation Lab. Report UCRL 2426, Rev. II.
27. Donlan, V. L. , "Computer Analysis of Proton Doses in Space," ASD-TDR-62-718, vol. 1, p. 171.
28. Wallace, R. , and C. Sondhaus, "Techniques Used in Shielding Calculations for High Energy Accelerators: Applications to Space Shielding," Proc. of Symposium on the Protection Against Radiation Hazards in Space, Gatlinburg, Tennessee, November 5-7, 1962, pp. 829-851.
29. Goldstein, H. , Fundamental Aspects of Reactor Shielding, Addison-Wesley, 1959, p. 30.
30. Evans, R. D. , The Atomic Nucleus, McGraw-Hill, 1955.
31. Peters, B. , "Progress in Cosmic Ray Research Since 1947," Journal of Geophysical Research, vol. 64, no. 2, February 1959, pp. 155-173.
32. Webber, W. R. , "An Evaluation of the Radiations Hazard Due to Solar Particle Events", Boeing Company, Report D2-90469, December 1963.

DOCUMENT CONTROL DATA - R&D

(Security classification of title, body of abstract and indexing annotation must be entered when the overall report is classified)

1. ORIGINATING ACTIVITY <i>(Corporate author)</i>		2a. REPORT SECURITY CLASSIFICATION	
The MITRE Corporation Bedford, Massachusetts		Unclassified	
		2b. GROUP	
		N/A	
3. REPORT TITLE			
Vulnerability of Manned Orbital Command Posts to Natural Space			
4. DESCRIPTIVE NOTES <i>(Type of report and inclusive dates)</i>			
N/A			
5. AUTHOR(S) <i>(Last name, first name, initial)</i>			
French, F. W. and Hansen, K. F.			
6. REPORT DATE		7a. TOTAL NO. OF PAGES	7b. NO. OF REFS
December 1964		86	32
8a. CONTRACT OR GRANT NO.		9a. ORIGINATOR'S REPORT NUMBER(S)	
AF 19(628)-2390		ESD-TDR-64-164	
b. PROJECT NO.		9b. OTHER REPORT NO(S) <i>(Any other numbers that may be assigned this report)</i>	
611.1		TM 4073	
c.			
d.			
10. AVAILABILITY/LIMITATION NOTICES			
Qualified requestors may obtain from DDC DDC release to OTS authorized			
11. SUPPLEMENTARY NOTES		12. SPONSORING MILITARY ACTIVITY	
		Directorate of Special Systems, Electronic Systems Division, L. G. Hanscom Field, Bedford, Massachusetts	
13. ABSTRACT			
<p>The shielding requirements for the protection of the crew of a manned orbital command post against the natural space radiations are investigated. Two types of orbits of military importance and of wide applicability are considered--a long-duration, high-altitude orbit above the Van Allen Belt and a short-duration, low-altitude polar orbit below it. Model environments for both orbits in terms of solar flare, cosmic, and Van Allen Belt radiations are postulated. Radiobiological tolerance criteria are investigated, and a somewhat unique criteria, based on partial recovery of sustained somatic damage, is proposed for the long duration mission.</p> <p>A mathematical description of the radiation transport of the separate environmental components through the radiation shield is formulated. Appropriate simplifications are used to obtain expressions for the doses due to primary protons, secondary protons and neutrons, and bremsstrahlung. Calculations are carried out on the IBM 7030 computer to obtain dose vs. thickness curves for different types and amounts of shielding material. These curves, together with the assumed model environment, and the postulated radiobiological tolerance criteria, are used to calculate minimum shielding thicknesses for both types of orbits. Conclusions are then drawn on the total amount of radiation shielding material that must be carried for each orbit.</p>			

14 KEY WORDS	LINK A		LINK B		LINK C	
	ROLE	WT	ROLE	WT	ROLE	WT
Shielding						
Shielding Manned Space Vehicle						
Mathematical Analysis						

INSTRUCTIONS

1. **ORIGINATING ACTIVITY:** Enter the name and address of the contractor, subcontractor, grantee, Department of Defense activity or other organization (*corporate author*) issuing the report.

2a. **REPORT SECURITY CLASSIFICATION:** Enter the overall security classification of the report. Indicate whether "Restricted Data" is included. Marking is to be in accordance with appropriate security regulations.

2b. **GROUP:** Automatic downgrading is specified in DoD Directive 5200.10 and Armed Forces Industrial Manual. Enter the group number. Also, when applicable, show that optional markings have been used for Group 3 and Group 4 as authorized.

3. **REPORT TITLE:** Enter the complete report title in all capital letters. Titles in all cases should be unclassified. If a meaningful title cannot be selected without classification, show title classification in all capitals in parenthesis immediately following the title.

4. **DESCRIPTIVE NOTES:** If appropriate, enter the type of report, e.g., interim, progress, summary, annual, or final. Give the inclusive dates when a specific reporting period is covered.

5. **AUTHOR(S):** Enter the name(s) of author(s) as shown on or in the report. Enter last name, first name, middle initial. If military, show rank and branch of service. The name of the principal author is an absolute minimum requirement.

6. **REPORT DATE:** Enter the date of the report as day, month, year; or month, year. If more than one date appears on the report, use date of publication.

7a. **TOTAL NUMBER OF PAGES:** The total page count should follow normal pagination procedures, i.e., enter the number of pages containing information.

7b. **NUMBER OF REFERENCES:** Enter the total number of references cited in the report.

8a. **CONTRACT OR GRANT NUMBER:** If appropriate, enter the applicable number of the contract or grant under which the report was written.

8b, 8c, & 8d. **PROJECT NUMBER:** Enter the appropriate military department identification, such as project number, subproject number, system numbers, task number, etc.

9a. **ORIGINATOR'S REPORT NUMBER(S):** Enter the official report number by which the document will be identified and controlled by the originating activity. This number must be unique to this report.

9b. **OTHER REPORT NUMBER(S):** If the report has been assigned any other report numbers (*either by the originator or by the sponsor*), also enter this number(s).

10. **AVAILABILITY/LIMITATION NOTICES:** Enter any limitations on further dissemination of the report, other than those

imposed by security classification, using standard statements such as:

- (1) "Qualified requesters may obtain copies of this report from DDC."
- (2) "Foreign announcement and dissemination of this report by DDC is not authorized."
- (3) "U. S. Government agencies may obtain copies of this report directly from DDC. Other qualified DDC users shall request through _____."
- (4) "U. S. military agencies may obtain copies of this report directly from DDC. Other qualified users shall request through _____."
- (5) "All distribution of this report is controlled. Qualified DDC users shall request through _____."

If the report has been furnished to the Office of Technical Services, Department of Commerce, for sale to the public, indicate this fact and enter the price, if known.

11. **SUPPLEMENTARY NOTES:** Use for additional explanatory notes.

12. **SPONSORING MILITARY ACTIVITY:** Enter the name of the departmental project office or laboratory sponsoring (*paying for*) the research and development. Include address.

13. **ABSTRACT:** Enter an abstract giving a brief and factual summary of the document indicative of the report, even though it may also appear elsewhere in the body of the technical report. If additional space is required, a continuation sheet shall be attached.

It is highly desirable that the abstract of classified reports be unclassified. Each paragraph of the abstract shall end with an indication of the military security classification of the information in the paragraph, represented as (TS), (S), (C), or (U).

There is no limitation on the length of the abstract. However, the suggested length is from 150 to 225 words.

14. **KEY WORDS:** Key words are technically meaningful terms or short phrases that characterize a report and may be used as index entries for cataloging the report. Key words must be selected so that no security classification is required. Identifiers, such as equipment model designation, trade name, military project code name, geographic location, may be used as key words but will be followed by an indication of technical context. The assignment of links, rules, and weights is optional.